NATURAL RESOURCES

GEOLOGIC MAP OF THE CHESTER MORSE LAKE 7.5-MINUTE QUADRANGLE, KING COUNTY, WASHINGTON

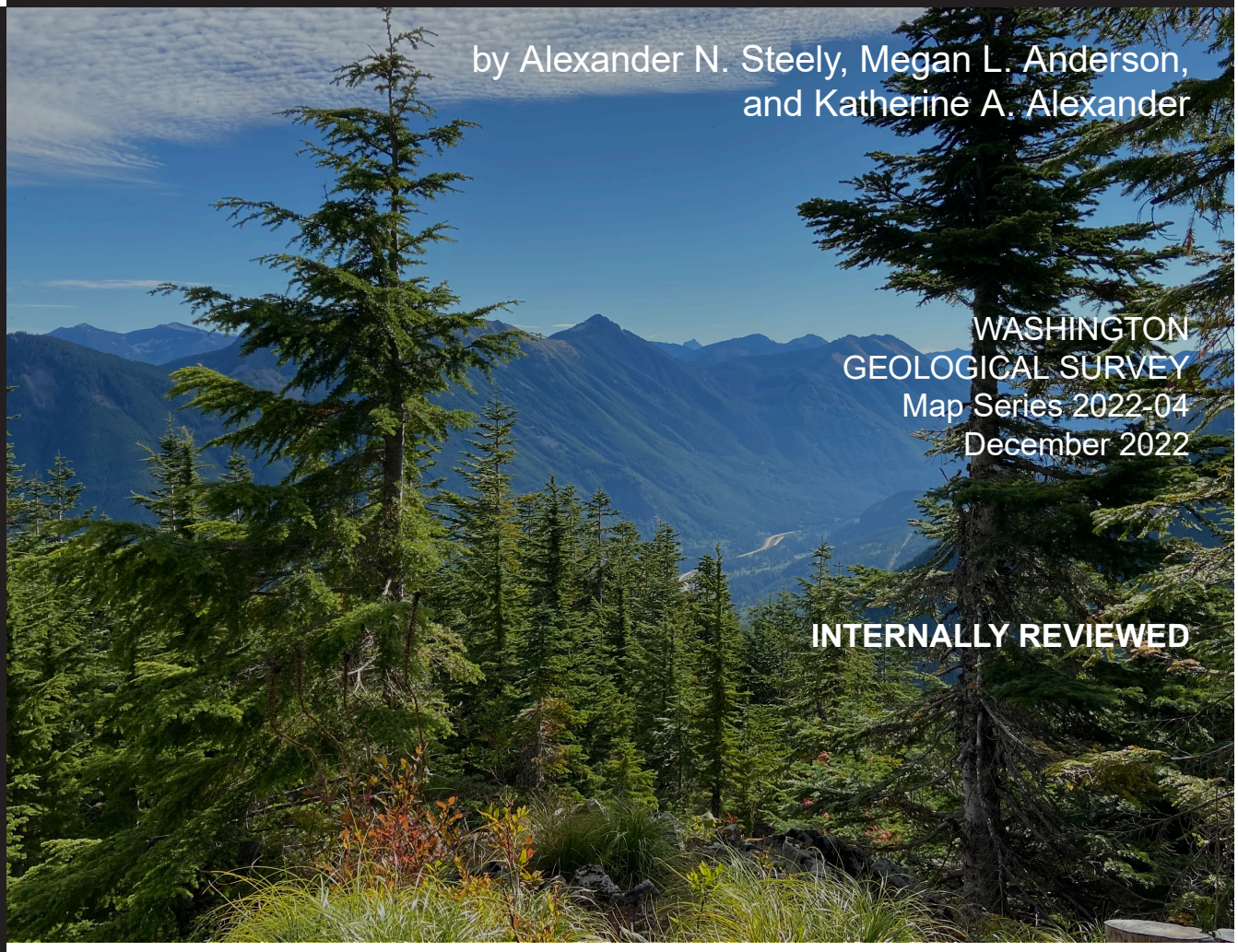

by Alexander N. Steely, Megan L. Anderson, and Katherine A. Alexander

WASHINGTON GEOLOGICAL SURVEY
Map Series 2022-04
December 2022

INTERNALLY REVIEWED

WASHINGTON STATE DEPARTMENT OF
NATURAL RESOURCES
WASHINGTON GEOLOGICAL SURVEY

GEOLOGIC MAP OF THE CHESTER MORSE LAKE 7.5-MINUTE QUADRANGLE, KING COUNTY, WASHINGTON

by Alexander N. Steely, Megan L. Anderson, and Katherine A. Alexander

WASHINGTON
GEOLOGICAL SURVEY
Map Series 2022-04
December 2022

This geologic map was funded in part by the USGS National Cooperative Geologic Mapping Program, award no. G21AC10798

This publication has been subject to an iterative technical review process by at least one Survey geologist who is not an author. This publication has also been subject to an iterative review process with Survey editors and cartographers.

WASHINGTON STATE DEPARTMENT OF
NATURAL RESOURCES
WASHINGTON GEOLOGICAL SURVEY

DISCLAIMER

Neither the State of Washington, nor any agency thereof, nor any of their employees, makes any warranty, express or implied, or assumes any legal liability or responsibility for the accuracy, completeness, or usefulness of any information, apparatus, product, or process disclosed, or represents that its use would not infringe privately owned rights. Reference herein to any specific commercial product, process, or service by trade name, trademark, manufacturer, or otherwise, does not necessarily constitute or imply its endorsement, recommendation, or favoring by the State of Washington or any agency thereof. The views and opinions of authors expressed herein do not necessarily state or reflect those of the State of Washington or any agency thereof.

INDEMNIFICATION

Research supported by the U.S. Geological Survey, National Cooperative Geologic Mapping Program, under USGS award number G21AC10798. The views and conclusions contained in this document are those of the authors and should not be interpreted as necessarily representing the official policies, either expressed or implied, of the U.S. Government.

WASHINGTON STATE DEPARTMENT OF NATURAL RESOURCES

Hilary S. Franz—*Commissioner of Public Lands*

WASHINGTON GEOLOGICAL SURVEY

Casey R. Hanell—*State Geologist*
Jessica L. Czajkowski—*Assistant State Geologist*
Ana Shafer—*Assistant State Geologist*

Washington State Department of Natural Resources
Washington Geological Survey

Mailing Address:
1111 Washington St SE
MS 47007
Olympia, WA 98504-7007

Street Address:
Natural Resources Bldg, Rm 148
1111 Washington St SE
Olympia, WA 98501

Phone: 360-902-1450
Fax: 360-902-1785
Email: geology@dnr.wa.gov
Website: http://www.dnr.wa.gov/geology

Publications and Maps:
www.dnr.wa.gov/programs-and-services/geology/publications-and-data/publications-and-maps

Washington Geology Library Searchable Catalog:
www.dnr.wa.gov/programs-and-services/geology/washington-geology-library

Suggested Citation: Steely, A. N.; Anderson, M. L.; Alexander, K. A., 2022, Geologic map of the Chester Morse Lake 7.5-minute quadrangle, King County, Washington: Washington Geological Survey Map Series 2022-04, 1 sheet, scale 1:24,000, 33 p. text. [https://www.dnr.wa.gov/publications/ger_ms2022-04_geol_map_chester_morse_lake_24k.zip]

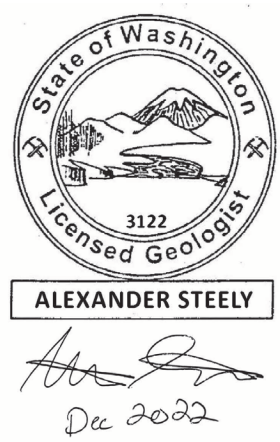

Contents

FIGURES

TABLES

MAP SHEET

Geologic Map of the Chester Morse Lake 7.5-minute Quadrangle, King County, Washington

by Alexander N. Steely[1], Megan L. Anderson[1], Katherine A. Alexander[1]

[1] Washington Geological Survey
1111 Washington St SE
MS 47007
Olympia, WA 98504-7007

ABSTRACT

We combine new geologic mapping, geochronology, geochemistry, thin-section analysis, a detailed gravity survey, and geophysical modeling to refine our understanding of the geology at the transition between the glaciated Puget Lowland and the volcanic and metamorphic Cascade Range in the Chester Morse Lake quadrangle.

Cretaceous to Jurassic rocks of the western mélange belt are the oldest in the area and consist of metasandstone (<86.5 Ma) and argillite interleaved with greenstone and meta-intrusive rocks (152–155 Ma). The contact with the overlying Tertiary rock is poorly exposed, but probably a faulted depositional surface above which a middle Eocene (<47.2 Ma) cherty conglomerate is locally present. The majority of Tertiary rock is a latest Eocene (~34.5 Ma) through Oligocene intermediate to silicic volcanic succession of thick crystal-vitric lapilli tuff and flows. Oligocene to Miocene mafic to felsic dikes and plutons, including the Snoqualmie batholith, are accompanied by a pronounced aureole of thermal metamorphism.

Late Quaternary units include abundant deposits from the last continental glaciation including thick accumulations of subglacial embankment deposits, which form the flat-topped surfaces near the mouths of major rivers and are mined for their aggregate. A now-incised series of fluvial deposits and terraces records the dynamic post-glacial adjustments as ice receded. There are isolated remnants of pre-glacial deposits and most are tilted and (or) faulted, though deformation associated with the advance of the Puget Lobe glacier in the most recent glaciation makes it difficult to deconvolve any older tectonic components. We find no compelling evidence for post-Vashon tectonic faulting.

INTRODUCTION

The Chester Morse Lake quadrangle is located in King County, about 55 km east of Seattle, at the transition between the glaciated Puget Lowland and the high topography of the volcanic and metamorphic Cascade Range (Fig. 1). The northern half of the quadrangle contains parts of both the Middle Fork Snoqualmie River and South Fork Snoqualmie River (hereafter referred to as 'Middle Fork' and 'South Fork'); Interstate 90 crosses the quadrangle and follows the South Fork canyon east toward Snoqualmie Pass. The Cedar River Watershed and Chester Morse Lake are located in the south half of the map area and are a protected water source for the city of Seattle (Fig. 1).

Access to the map area is good, although there are still significant challenges. In the north half of the quadrangle, suburban development in the low areas has left few vestiges of the underlying geology. In undeveloped areas logging roads are sparse, but hiking trails are abundant; the quadrangle contains trail systems on the south flank of Mount Si, near Mailbox Peak, and throughout Olallie State Park. These trail systems provide the best access to rock exposures in the quadrangle. In the Cedar River Watershed, the city of Seattle maintains a network of roads that were previously used for logging, though some areas are inaccessible because approximately half of the old roads have been decommissioned.

The intention of this new map is to improve our understanding of the geologic history of Washington, better understand the geologic setting of earth and water resources, and assist in the identification and characterization of geologic hazards. Understanding the seismic risk in this area is crucial—nearly 3 million people (almost half of the State's population) live within the extent of Figure 1. Many homes and buildings, including schools and hospitals, are constructed on liquefaction-prone unconsolidated deposits. There are also six large reservoirs in the nearby foothills, which are used for both flood control and for drinking water in Seattle, Tacoma, and nearby cities, and all of the reservoirs were built before the recognition of major nearby active faults. This map builds upon a multitude of previous studies, notably those of Dragovich and others (2009a), Tabor and others (2000), Hammond (1963), and Fuller (1925).

GEOLOGIC OVERVIEW

A diverse assemblage of glacial deposits blankets most of the low topography in the map area. These deposits are a result of the interaction between voluminous Cascade Range river systems and the advance and retreat of Pleistocene continental glaciers (Booth, 1990). The oldest bedrock is Mesozoic low- to

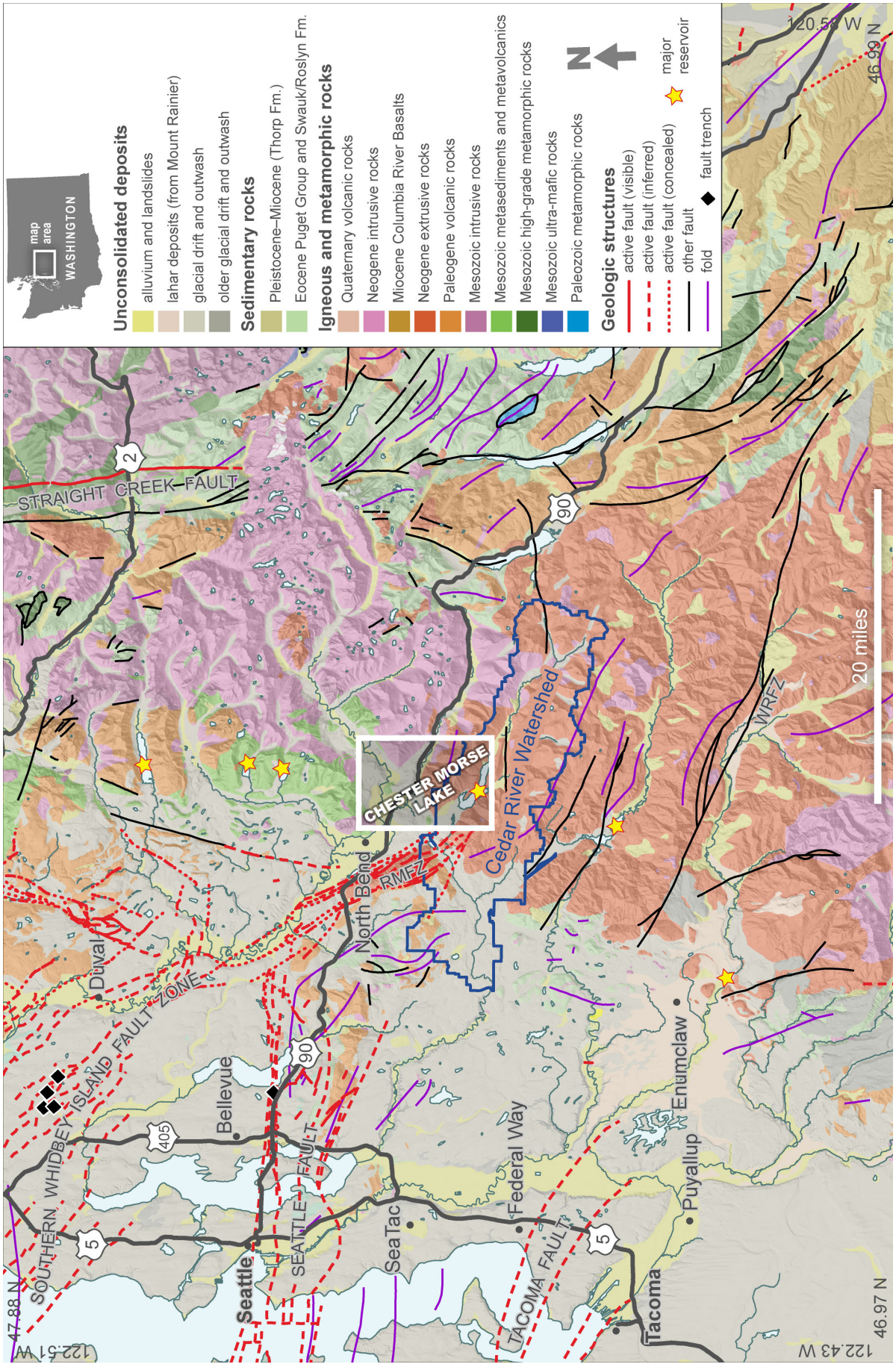

Figure 1. Regional geology and tectonic setting near the Chester Morse Lake quadrangle.

medium-grade metamorphic rocks of the western mélange belt (Frizzell and others, 1987; Tabor and others, 1993, 2000). These rocks have a complicated Jurassic to Cretaceous history and were accreted to Washington in the late Cretaceous or Paleocene (for example, Tabor and others, 2000). Eocene continental sedimentary and volcanic rocks of the Puget Group overlie these older rocks. Thick Neogene volcanic and volcaniclastic rocks crop out in the area and are the remains of the ancestral Cascade Range volcanic arc (Tabor and others, 2000). These volcanics and the older metamorphic rocks are intruded by the early Miocene Snoqualmie batholith and various smaller Oligocene and Miocene felsic–intermediate intrusions (Tabor and others, 2000).

Two major active fault systems converge near the project area (Fig. 1): the reverse-slip east-striking Seattle Fault and the oblique-slip northwest-striking southern Whidbey Island fault zone (SWIF). Together these two systems (and other associated faults, like the Rattlesnake Mountain fault) accommodate northward shortening in the forearc of the Cascadia subduction zone (Wells and others, 1998), but their kinematic linkage remains uncertain. The Seattle Fault was the source of a large earthquake circa A.D. 950. The fault has ~8–10 km of total offset across it (Liberty and Pratt, 2008; ten Brink and others, 2002), has produced a topographically high bedrock-cored antiform in its hanging wall, and is associated with abundant seismicity at shallow and mid-crustal depths (Dragovich and others, 2009a,b). There is also abundant seismicity near the SWIF, which has a history of Holocene rupture (Sherrod and others, 2008), but the SWIF has a greater proportion of strike-slip movement than the Seattle Fault. These faults strike toward the Cascade Range—and towards active faults of the western Yakima fold and thrust belt—and this has led to much speculation about how (or if) there is a through-going fault connection (Blakely and others, 2011).

Geologic maps at 1:24,000 scale northwest of the map area were largely completed with the intent of understanding the Seattle Fault and SWIF (Dragovich and others, 2007, 2009a,b, 2010, 2012). To the southwest there is additional 1:24,000-scale mapping of older vintage that focused on the coal resources within the Eocene rocks and the overlying glacial cover (Crandell, 1963; Mullineaux, 1965; Vine, 1969). Other foundational work in the area is a 1:100,000-scale map prepared by Tabor and others (2000), which consolidated observations from many unpublished efforts and theses to map the volcanic rocks of the ancestral and present Cascade Range. Paleoseismic studies (for example, Sherrod and others, 2008), active-seismic imaging (for example, Brocher and others, 2004; Liberty and Pratt, 2008), and structural geology studies (for example, Kelsey and others, 2008) also form an extensive body of relevant knowledge, but are focused mainly to the west. Work by Hammond (1963) was built on the pioneering studies of Smith and Calkins (1906) and Fuller (1925) and provides a solid basis for understanding the volcanic rocks of the Cascade Range, the metamorphic bedrock upon which the volcanics rest, and the intrusive rocks of the region.

METHODS

The geologic map is based on field observations collected during the summer and fall of 2021 using standard geologic field techniques. During field work, we described rocks and deposits, measured the attitudes of bedding, faults, fractures, and folds, and collected samples for analytical work or later characterization. We recorded all data on a tablet or phone using Esri's ArcGIS Collector. We augmented the field data with lidar (King County, 2003; PSLC, 2014, 2016), and data from publicly available water-well records and subsurface borings from the Washington Department of Ecology. We used these data to develop a 1:24,000-scale geologic map using ArcGIS. Two cross sections illustrate subsurface relationships, and a correlation of map units indicates the relative ages of the rocks and deposits. From our field observations—and the other data collected and discussed below—we wrote detailed descriptions of the mapped units and compiled this and any other relevant observations and interpretations into this pamphlet.

We adopt the alluvial fan and landslide mapping of Mickelson and others (2019), generally without modification; exceptions are noted as follows. A few polygon edges were moved less than ~10 m to avoid narrow slivers between adjacent landslides or alluvial fans. To satisfy the topology of our geologic maps, overlapping landslide polygons (where younger landslides lie on top of older landslides) are shown as separate polygons without any overlap. All alluvial fans in the Cedar River Watershed are from our mapping.

During our mapping we collected ~750 new observations, including 170 new measurements of bedding, flow foliation in volcanic units, and compaction or shear foliation in metamorphic units. We also compiled some bedding and foliation measurements from Tabor and others (2000) and Hammond (1963). Compiled data are noted in the GIS and are placed according to the original author, except where noted, and thus may appear to be located in a geologic unit different than that in which they were originally mapped. In volcanic units we used the 'bedding' symbol where we measured an orientation between two different lithologies (for example, between a flow and a tuff) and the 'flow foliation' symbol where we measured an orientation that lacks a change in lithology. Due to scale, not all attitudes are shown on the map plate, but all are included in the GIS data. We collected 31 new observations of fault surfaces and found kinematic data at 11 of these sites; both fault and slickenline orientations are shown on the map. We also collected 34 samples for thin sections, which are used to help differentiate between different types of fine-grained metamorphosed rocks and to aid in characterizing rock units and mineralogy. At two sites we collected and described about 50 clasts from pebble-bearing units and these data are used to understand provenance.

To determine the crystallization age of intrusive rocks and volcanic tuffs and flows, we analyzed seven samples using the $^{40}Ar/^{39}Ar$ method and four samples using the U-Pb method on zircon; we used both methods on one sample. We also analyzed two samples for detrital zircon U-Pb to constrain age and provenance. We collected and analyzed four luminescence samples and two ^{14}C samples to constrain the ages of Pleistocene deposits; one ^{14}C sample is compiled from Fairhall and others (1966) and relocated. Lastly, we analyzed the major- and trace-element geochemistry for eight of the dated samples. Summary results are in Table 1; analytical methods and sample information are

in Appendix A and Appendix B; detailed tabular data are in the Data Supplement.

We also collected and interpreted 304 new gravity measurements—in addition to existing aeromagnetic data from Blakely and others (1999)—to help constrain the location and subsurface geometry of faults and geologic units (Fig. M1). New gravity data have 1-km grid spacing where possible and 250-m spacing along the cross section line. To avoid edge effects in the new gravity map, we collected data beyond the edge of the map area. The refined gravity map includes 145 new gravity observations within the map area, 159 new points outside of the map area, and three points from previous studies (Finn and others, 1991).

Modeled isostatic gravity and aeromagnetic profiles (using GM-SYS; Geosoft, Inc.) along Cross Section X–X′ (Fig. M1B) quantitatively test subsurface interpretations developed from qualitative interpretations of map-view data. Rock density and magnetic susceptibility measurements of samples from 53 outcrops within and just outside the map area help constrain these models. These geophysical data and analyses supplement our geologic interpretations. Appendix C contains details of gravity, magnetic, rock property, and modeling methods; tabular data are in the Data Supplement.

We report our measurements and data using the metric system; the one exception is elevation, which we report in feet-above-mean-sea-level (ft) to aid in comparison with topographic maps.

DESCRIPTION OF MAP UNITS

Holocene Nonglacial Deposits

af **Artificial fill (Holocene)**—Mixed earth materials of varied grain size and sorting placed to elevate the land or modify topography; may contain organic material, concrete, or debris; may be engineered; loose to compact; shown where thick and (or) extensive; differentiated from modified land by greater thickness and a composition that differs from that of the underlying geologic unit. Mapped predominantly along Interstate 90, other major roads, and in a large gravel storage area just west of Grouse Ridge.

ml **Modified land (Holocene)**—Mixed earth materials of varied grain size and sorting; modified by humans; typically modifies other unconsolidated deposits; may contain organic material, concrete, or debris; may be engineered; loose to compact; shown where thick and (or) extensive; differentiated from artificial fill by a composition that matches the underlying geologic unit though where other original characteristics (such as bedding) are no longer recognizable.

Qa **Alluvium (Holocene)**—Gravel, sand, silt, and clay, in varied abundance; locally contains scattered boulders, some greater than 5 m across; well to poorly sorted; may be stratified or contain other sedimentary structures; locally contains organic material and (or) soil; generally loose. Unit is mapped where there is at least some evidence of geologically recent fluvial deposition or erosion; as such it is found along the major perennial streams and rivers. Unit thickness is as thin as ~2 m along smaller streams, but is substantially thicker in the broad valley of the Middle Fork where it could be many tens of meters thick. The unit is considered Holocene, but may locally contain deposits as old as late Pleistocene in the glaciated uplands. Where unit Qao is present, unit Qa is topographically lower and (or) inset into unit Qao. The largest boulders in this unit are found in the active stream channel, and are especially abundant near where the Middle Fork and South Fork incise into the thick, boulder-rich deposits of unit Qgd. It seems reasonable that the boulders were eroded from these adjacent deposits because they may be too large to be mobile under modern river conditions. We suspect that the river incises and aggrades around these outsized clasts, thus concentrating them near their source.

Qao **Alluvium, older (Holocene)**—Gravel, sand, silt, and clay, in varied abundance; locally contains scattered boulders; well to poorly sorted; may be stratified or contain other sedimentary structures; locally contains organic material and (or) soil; generally loose. Unit is mapped adjacent to major perennial streams and rivers except where evidence for geologically recent fluvial deposition or reworking is absent; the top of the deposit is typically several meters above the stream channel. Although not present everywhere, there is typically a lower, inset deposit (unit Qa) between the stream or river and deposits of unit Qao. The unit varies from ~2–20 m thick and is considered Holocene. Deposits of this unit mapped above ~1,100 ft elevation along the South Fork lack continuity with unit Qao downstream and might correlate with units $Qgoa_1$ or $Qgoa_2$ instead, though they are mapped as unit Qao because they are only a few meters above the modern river.

Qb **Beach and nearshore deposits (Holocene)**—Sand, locally interbedded with varying amounts of silt and clay; scattered pebbles to boulders are locally common. Mapped along the shores of Chester Morse Lake and Masonry Pool.

Qp **Peat (Holocene)**—Organic-matter-rich silt to clay; locally sandy; typically loose and easily compacted; includes peat, muck, and gyttja; deposited in low-energy fluvial environments and closed depressions such as bogs, swamps, abandoned river channels, kettles, and lakes; commonly contains abundant fibrous or woody plant debris.

Qct **Colluvium and talus (Holocene)**—Boulders, cobbles, pebbles, sand, silt, clay, soil, organic material, and semi-intact blocks of older deposits or bedrock,

Table 1. Summary of geochronology and co-located samples. Uncertainties are provided at 2-sigma (95%) confidence.

Map ID	Interpreted geologic unit	Dating method	Age	Age type	Material	Co-located analyses	Geochemical classification*
GD1	Qgoa2	^{14}C	7,160 ±30 14C yr BP	Maximum depositional age	charcoal	– – –	– – –
GD2	Jiw	U-Pb	155.79 ±0.35 Ma	Crystallization	zircon	TS3	– – –
GD3	Qguc	Luminescence	21.5 ±1.6 ka	Burial	feldspar	– – –	– – –
GD4	Qguc	Luminescence	40.0 ±3.4 ka	Burial	feldspar	– – –	– – –
GD5	MOii	$^{40}Ar/^{39}Ar$	21.01 ±0.10 Ma 24.80 ±0.08 Ma 25.24 ±1.01 Ma	Cooling? Crystallization Crystallization	plagioclase biotite groundmass	G1; TS8	Gabbro
GD6	Qguc	Luminescence	42.3 ± 4.7 ka	Burial	feldspar	– – –	– – –
GD7	Qguc	Luminescence	49.1 ±5.4 ka	Burial	feldspar	– – –	– – –
GD8	KJmsw	U-Pb	<86.54 ±0.96 Ma	Detrital; maximum depositional age	zircon	– – –	– – –
GD9	OEv (tuff)	$^{40}Ar/^{39}Ar$	22.86 ±0.05 Ma	Cooling	groundmass	GD10; G2; TS11	Dacitic rhyolite
GD10	OEv (tuff)	U-Pb	34.66 ±0.10 Ma	Crystallization	zircon	GD9; G2; TS11	Dacitic rhyolite
GD11	Qgl	^{14}C	9,140 ±30 14C yr BP	Maximum depositional age	charcoal	– – –	– – –
GD12**	Qgl	^{14}C	13,570 ±130 14C yr BP	Maximum depositional age	unknown	– – –	– – –
GD13	Jiw	U-Pb	152.97 ±0.34 Ma	Crystallization	zircon	G3	Gabbro
GD14	OEv (tuff)	$^{40}Ar/^{39}Ar$	28.72 ±0.08 Ma	Crystallization?	groundmass	G4; TS20	Andesite
GD15	Ecg	U-Pb	<47.20 ±0.39 Ma	Detrital; maximum depositional age	zircon	TS21	– – –
GD16	OEv (tuff)	U-Pb	34.47 ±0.09 Ma	Crystallization	zircon	– – –	– – –
GD17	OEv (flow)	$^{40}Ar/^{39}Ar$	31.91 ±0.07 Ma	Crystallization?	groundmass	G5; TS25	Andesite
GD18	OEv (flow)	$^{40}Ar/^{39}Ar$	32.90 ±0.17 Ma	Crystallization?	groundmass	G6; TS27	Basaltic andesite
GD19	OEv (flow)	$^{40}Ar/^{39}Ar$	18.44 ±0.05 Ma	Cooling	groundmass	G7; TS30	Basaltic trachyandesite
GD20	OEv (tuff)	$^{40}Ar/^{39}Ar$	25.60 ±0.08 Ma	Cooling	groundmass	G8; TS33	Dacite

*Using the Total-Alkali-Silica diagram of LeMaitre and others (2002).

**Sample UW-35 from Fairhall and others (1966).

in varied abundance; clast to matrix supported; clasts range from angular to rounded, depending on source material; loose to compact. Includes deposits from small debris flows, topples, rock avalanches, talus, scree, and colluvium. May include deposits from small, unmapped shallow landslides. Thickness is poorly constrained but likely varies from ~1–10 m; some talus slopes have been quarried for road material and are greater than 15 m thick. Unit Qct is widespread in the map area and is most prevalent on the mountainous slopes south of Interstate 90, where it varies from soil-rich forested slopes to barren talus fields. The unit is interpreted to be largely Holocene but may locally include some deposits from the late Pleistocene, especially in glaciated uplands. This unit locally contains outcrops of other units too small to be mapped separately.

Qls **Landslide (Holocene)**—Boulders, cobbles, pebbles, sand, silt, clay, soil, organic material, and semi-intact blocks of older deposits or bedrock, in varied abundance; typically matrix supported; generally unsorted; clasts angular to rounded, depending on source material; loose to compact. May include deposits from both shallow (depth less than that of tree roots) and deep-seated landslides, debris flows, topples, and rock avalanches. Thickness is often poorly constrained and varies from a few to several tens of meters, but may locally be much thicker. Unit Qls is interpreted to be largely Holocene but probably includes some deposits from the late Pleistocene, especially in glaciated areas. Landslides are entirely from Mickelson and others (2019). Absence of a mapped landslide does not indicate the absence of landslide hazard.

Qaf, Qafo **Alluvial fan (Holocene)**—Pebble to boulder gravel and sand in varied abundance; moderately to poorly sorted; stratification varies from absent to weakly planar bedded; may contain organic material and (or) soil; typically somewhat compact to loose. Unit is mapped along and adjacent to streams where they emerge from confined channels into broader and flatter topography. Unit is differentiated from other Holocene units primarily based on the presence of fan-shaped surface morphology. Alluvial fans mapped outside of the Cedar River Watershed are from Mickelson and others (2019); those within the watershed are from this study. Unit Qafo is mapped only near Cedar Butte and in one location along the Middle Fork where undissected alluvial fans (unit Qaf) appear to be deposited on top of dissected fan-shaped surfaces (unit Qafo). Unit Qafo is from this study and was not mapped by Mickelson and others (2019).

Late Pleistocene Glacial and Nonglacial Deposits

The most recent continental glaciation in the Puget Lowland occurred during the Vashon stade of the Fraser glaciation. The glaciation had a profound effect on the landscape of the region, and was quite rapid; the glacier, known as the Puget Lobe, advanced past the latitude of Seattle about 15 ka and was gone by about 13.5 ka (Booth and Goldstein, 1994). As the glacier advanced southward, it blocked rivers draining the Cascade Range, commonly forming ice-margin lakes and subglacial rivers (Porter, 1976; Booth, 1986). The advancing glacier also scoured the land and removed much of the pre-glacial stratigraphy (Booth, 1994). This scouring is also accompanied by deformation of pre-glacial deposits, and can make distinguishing between ice-related deformation and tectonic deformation difficult.

During the non-glacial time prior to the arrival of the Puget Lobe glacier, most of the Puget Lowland likely looked similar to the modern environment, with rivers depositing alluvium in valleys inset into older glacial deposits. Evidence in the Cascade Range indicates that alpine glaciers were present before and after the Puget Lobe advanced and retreated, but there is no evidence that the two types of glaciers interacted (Porter, 1976).

In much of the Puget Lowland, deposits from the Puget Lobe contain potassium-feldspar-bearing granitoids and high-grade metamorphic rocks. These lithologies could only have been transported into the southern Puget Lowland by an advancing continental ice sheet from the Canadian Cordillera and northernmost Washington. However, such lithologies are rarely found in glacial deposits within the map area, perhaps because they are overwhelmed by material carried by ice-marginal river systems.

DEPOSITS OF LOCAL RIVERS DURING GLACIAL RECESSION

As the Puget Lobe glacier thinned and receded, a series of subaerial spillways were uncovered and formed sills for glacial lakes (Bretz, 1913). The first of these was the Cedar Spillway at 930-ft elevation—near the present-day location of Rattlesnake Lake—that created Glacial Lake Snohomish (Mackin, 1941; Thorson, 1981). Continued glacial recession uncovered a lower spillway, rapidly lowering the lake level to the new sill at 520 ft; this lake is called Glacial Lake Sammamish (Porter, 1976; Thorson, 1981). Booth (1990) and Tabor and others (2000) map a series of successively lower and younger 'recessional outwash' deposits near the map area that record the lowering base level of these glacial lake systems. During this time, local rivers (which lack Puget Lobe glacial meltwater) interacted with the voluminous glacial meltwater from the Puget Lobe. Because discharge volume, sediment flux, and source area differ markedly between the two potential sources of sedimentary deposits, we use the terms 'old alluvium' for fluvial deposits of local rivers formed during glacial recession and 'outwash' for similarly aged deposits resulting from glacial meltwater. In this area we differentiate two ages of old alluvium on the basis of geomorphology, elevation, and inset relationships; a younger unit below 930-ft elevation (unit $Qgoa_1$), and an older unit above 930 ft elevation (unit $Qgoa_2$).

$Qgoa_1$ **Old alluvium (Holocene to late Pleistocene)**—Cobble and boulder gravel to coarse sand with

subordinate silt; scattered, outsized boulders are up to 5 m across; well to poorly sorted; typically crudely stratified or structureless, but where stratified locally has well-developed planar bedding or low-angle cross stratification; varies from angular to well rounded, commonly within a single exposure; sand is typically more angular than larger clasts; ranges from loose to moderately consolidated; exposed in cut banks along major rivers; greater than 100 m thick north of Grouse Ridge. Well-developed flat benches are locally common and their back edges are marked by a steep riser; these features are interpreted as cut-and-fill terraces. West and south of Grouse Ridge, unit Qgoa$_1$ is mapped below ~930 ft elevation where smooth and flat surfaces lie adjacent to major rivers and into which units Qa and Qao are inset. Upstream of Grouse Ridge we map unit Qgoa$_1$ by tracing flat benches from the ~930-ft level, providing for an upstream gradient of between 3.8–4.8 m/km, similar to the gradient of the modern river.

The ~930-ft elevation is important because it is about the elevation of Glacial Lake Snohomish, which filled the Snoqualmie River valley during early stages of glacial recession (Mackin, 1941; Thorson, 1981). A steep (up to 35 m/km) fan-shaped deposit—mapped as unit Qgoa$_1$—heads at this elevation at the north end of Grouse Ridge and likely grades to the 520-ft elevation of Glacial Lake Sammamish (Porter, 1976; Thorson, 1981) near the edge of the map area. Thus the unit, as mapped and interpreted, post-dates Glacial Lake Snohomish, and at least the oldest (and highest) portions of the unit are the same age as Glacial Lake Sammamish. The flight of inset benches and deposits mapped in unit Qgoa$_1$ descend nearly to the modern river level and record further base-level lowering into and through the Holocene.

Qgoa$_2$ **Old alluvium (Pleistocene)**—Cobble and boulder gravel to coarse sand with subordinate silt and, locally, minor lenses of diamicton; scattered outsized boulders are up to 5 m across; well to poorly sorted; typically crudely stratified or structureless; where stratified, locally has well-developed planar bedding or low-angle cross stratification; varies from angular to well rounded, commonly within a single exposure; sand is typically more angular than larger clasts; ranges from loose to compact; exposed in cut banks along major rivers and along steep valley walls. Well-developed flat benches are locally common and their back edges are marked by a steep riser; these features are interpreted as cut-and-fill terraces.

This unit is mapped above 930-ft elevation where sediment is inferred to have been deposited by local rivers and not glacial meltwater of the Puget Lobe. Unit Qgoa$_2$ was likely deposited, at least in part, at the same time as glacial outwash (units Qgo and Qgik) in the map area. A broad, nearly delta-shaped outcrop belt of unit Qgoa$_2$ is mapped near the mouth of the South Fork; the southern portion of this belt appears to correlate with units Qgo and Qgik near Cedar Butte and could indicate that stagnant ice blocked westward flow of the river, diverting it south into the Cedar River. The northern (and lower) portion of this outcrop belt has unusually muted topography and might indicate either deposition into, or modification by, Glacial Lake Snohomish. A radiocarbon age on charcoal of 7,160 ^{14}C yr BP (age site GD1, elevation of 1,172 ft) near Granite Creek along the Middle Fork seems far too young for this unit. We suspect that the fine-grained debris flow from which this sample was collected may be a younger deposit inset into unit Qgoa$_2$ instead of a debris flow within the old alluvium.

DEPOSITS OF THE VASHON STADE OF THE FRASER GLACIATION

Qgb **Beach and nearshore deposits (Pleistocene)**—Sand, silt, and minor gravel in varied abundance; poorly exposed and mapped predominantly on the basis of geomorphology. A subtle shoreline is mapped at ~1,630 ft elevation north of Masonry Pool near the mouth of the Cedar River canyon; north and west of this boundary there is a low-amplitude topographic ridge with a series of inset northwest-trending ~4–10-ft-tall low-gradient topographic steps that were interpreted by Mackin (1941) as fluvial channels; south and east of the shoreline there are no such steps and the land slopes gently south to Masonry Pool and then east toward Chester Morse Lake; alluvial fans appear to be deposited on top of this gently sloping surface. We interpret these observations as the geomorphic expression of a lake that was impounded by deposition of units Qgd and Qgik across the mouth of the Cedar River canyon. The maximum elevation of this lake is constrained by the ~1,640 ft elevation of unmodified unit Qgik deposits near the dam for Masonry Pool. We suspect that there is a thin, perhaps discontinuous, blanket of lacustrine deposits above unit Qgd where we map this unit, but did not find convincing evidence in the few exposures along the shore of the modern reservoirs; elsewhere thick soil and forest do not provide exposure of the underlying deposits. We do not know the length of time this lake was at the 1,630 ft elevation, nor whether the smooth topography below the shoreline is a result of deposition and infilling or erosion as the lake level dropped. Cedar Lake (the natural precursor to man-made Chester Morse Lake) was at an elevation of 1,530 ft (Mackin, 1941) prior to building any dams, which, coupled with evidence for a glacial lake, indicates that lakes have been a persistent feature in this valley throughout the Holocene and at least intermittently

in the Pleistocene. However, the deposits of unit Qgb are well above the known Holocene elevation of Cedar Lake and we suspect that they are late Pleistocene in age.

Qgo **Outwash, recessional (Pleistocene)**—Gravel, sand, and minor(?) silt in varied abundance; typically tan; loose to consolidated; well bedded to structureless; sandy and silty intervals are generally well sorted; gravelly intervals are generally moderately to poorly sorted and typically clast supported; subangular to rounded grains and clasts; cursory lithologic characterization (due to lack of outcrop) indicates a variety of plutonic, metamorphic, and volcanic rock types consistent with bedrock geology in the eastern portions of the Cascade Range, but does not preclude nor require a provenance outside of the region. Subrounded boulders of plutonic rock up to several meters across are found on the surface, though it is not clear if these were deposited on the surface or are weathering out of the deposit. There are few exposures of this unit and so its extent is largely inferred from geomorphic evidence and scattered observations. Unit thickness is probably less than 100 m, but is difficult to constrain: we infer about 90 m in thickness from the change in elevation between the base to the top of the unit at Tanner butte and north of Cedar Butte; a well from a high portion of Tanner butte (water well W16) records ~84 m of sand and gravel (including many boulders), but north of Cedar Butte, bedrock is found at shallow depth in wells (water wells W33–35).

The two large expanses of this unit (south from Tanner butte and north of Cedar Butte) have a smooth and subtly stepped surface that contrasts with the dimpled surface of unit Qgic (which typically lies adjacent to and below unit Qgo). These steps could be shorelines from an early stage glacial lake, but they are well above the 930 ft elevation of the Cedar Spillway. If such a lake existed, then the boulders now resting on the surface might have been deposited by melting ice rafts. The steps could also be fluvial terraces related to a lowering of base level as the ice receded. In either case, the narrow extent of unit Qgo along Tanner butte and the mostly fresh appearance of unit Qgic on either side suggest that unit Qgo was probably deposited in a narrow, ice-bound valley, instead of being deposited more extensively and then eroded. A flat-topped deposit of unit Qgo is mapped through a narrow gap between Cedar Butte and the western flank of Mount Washington and is slightly lower in elevation than an unpaired set of terraces that we interpret as kame deposits (unit Qgik); thus, unit Qgo may post-date some kame terraces, but in other places unit Qgo is likely correlative with them.

Qgd **Glacial embankment deposits (Pleistocene)**—Sand and gravel in varied amounts, with sparse pebble to boulder diamicton (till) and minor interbedded clayey silt; organic-rich beds are rare; generally light tan to light gray, with little weathering of clasts or matrix; till and silt are compact and dense; sand and gravel are moderately to weakly consolidated and generally thinly to thickly bedded; sorting varies, from unsorted matrix-supported till, to well-sorted and well-bedded finer-grained deposits. Clasts are mostly subrounded to rounded, some are faceted, and there are many boulders >5 m across. Till layers are several meters thick and locally pinch out; intervals of sand and gravel are commonly tens of meters thick. Unit Qgd is at least 290 m thick along the Middle Fork near Mine Creek, where the base of the unit contains a dense, 1-m-thick organic-rich bed above ~10 m of sand and gravel that, in turn, overlies unit Qgl. At least 200 m of unit Qgd is found in the canyon of the South Fork (where it overlies unit Qguc).

Smooth and gently east-dipping surfaces cap these deposits, form prominent topographic features in the area, and are a defining geomorphic feature of the 'embankment deposits'. The embankments are found at the mouth of each major river. Subtle inset channels are found on the surface of the deposits: those on the Middle Fork and South Fork embankments are both ~13 m deep, 100–220 m wide, and descend eastward to delta-shaped surfaces just under 1,600 ft elevation; slopes range from 3–10 m/km. The channels on the Cedar River embankment are more numerous and subtle than those farther north, and are obscured below ~1,630 ft elevation by unit Qgb. Booth (1986) interprets these deposits as resulting from sub-glacial accumulation of sediment near the ice grounding line during glacial maximum. This dynamic environment is envisioned to have basal till deposits that complexly interfinger with sub-glacial delta deposits, that in turn interfinger and grade into sub-glacial lacustrine deposits and water-lain till. Unit Qgd is differentiated from unit Qgic by its greater thickness, flat-topped surface, lack of stagnant-ice surface morphology, and much higher proportion of fluvial deposits.

Qgic **Ice-contact deposits (Pleistocene)**—Varied assortment of diamicton (till) and stratified to structureless sand to cobble and boulder gravel; generally light gray to light tan with little weathering of clasts or matrix; diamicton is compact and typically consists of unsorted lenses of silt to clay matrix with dispersed pebbles to large boulders up to several meters thick; stratified deposits are less compact and locally loose, up to a few tens of meters thick, and contain poorly to well-sorted mixtures of subrounded sandy gravel to coarse boulder gravel; sand grains are characteristically less rounded than pebbles and cobbles. Clast lithologies are varied and include a wide range of plutonic and metamorphic rocks with few volcanic rocks. We interpret the interbedding

of till lenses and stratified deposits as generally indicating deposition near a fluctuating glacial-ice margin. Where this unit is mapped directly west of the large embankment deposits (unit Qgd), we interpret it as grounded-ice deposits after Booth (1986). Because the grounding line of the Puget Lobe likely varied through time (Booth, 1986), we suspect that till from this unit has a complex, probably interfingering relationship with unit Qgd, and that mapping them as two separate units is likely a drastic simplification. The surface of unit Qgic is typically dimpled, without directional fabric, and locally contains outsized boulders at the surface. We interpret these features as having formed by melting stagnant ice during glacial recession, which suggests that throughout much of this map area, the Puget Lobe ice did not retreat so much as melt in place.

Qgt **Lodgement till (Pleistocene)**—Diamicton and minor stratified sand or gravel; typically light to dark gray, with mild weathering of clasts or matrix; compact; generally consists of silt to clay matrix with dispersed sparse to abundant pebbles, cobbles, and boulders; clasts are generally subrounded and some are faceted; typically lacks fabric, but locally there is weakly developed friable and subhorizontal layering. Clast lithologies are varied and include a wide range of plutonic and metamorphic rocks with few volcanic rocks. This unit is mapped where it is particularly thick or extensive, and (or) where it is found to separate pre-glacial deposits (units Qgl or Qguc) or bedrock from glacial deposits. Lenses of till, and perhaps thicker accumulations, are present in units Qgic, Qgd, and to a lesser extent in unit Qgik, though these lenses are too small to be mapped separately. Springs and seeps are common at the top of this unit.

Qgik **Kame deposits (Pleistocene)**—Pebble to boulder gravel, pebbly sand, and minor compact diamicton; generally light tan to light gray; mildly weathered; typically loose to somewhat consolidated; typically stratified, mostly consisting of medium to thick planar bedding, but locally structureless; clasts are subangular to subrounded; generally moderately sorted. Mapped near the mouth of the Cedar River where a flight of unpaired terraces are above a dimpled surface of unit Qgic and are inset into the embankment deposit at the river canyon's mouth; here we interpret unit Qgik to reflect an ice-marginal river system during glacial recession but before establishment of the Cedar Spillway (which is nearly 600 ft lower in elevation than unit Qgik); these deposits are probably only a few tens of meters thick. The unit is also mapped south of Mount Si and Mount Teneriffe, where terraced deposits on the steep mountain slopes are found up to an elevation of ~2,050 ft and may be as thick as 170 m. Here the deposits contain a larger proportion of angular and sub-angular clasts and a more variable amount of weathering than seen to the south, including clasts that are relatively fresh and rarer clasts that are decomposed and friable. Compared to the maximum height of the embankment deposits a few kilometers to the east, the lower portions of unit Qgik in this area are at about the same elevation, but the upper surfaces are about 370 ft higher. One outcrop at ~1,800 ft elevation just north of the map area along the Mount Teneriffe trail exposed a dark brown and very compact angular-clast diamicton. Based on its height and the moderate amount of weathering, it is possible that this outcrop could be pre-Vashon in age. Regardless of age, it seems that unit Qgik along the mountain front here is likely the remnant of an ice-marginal river system trapped between the ice and the high topography, but it is not clear if these deposits were subaerial or subglacial. The queried unit Qgik directly south of Mount Teneriffe has an upper elevation similar to unit Qgd just to the east, and could instead be an outcrop of that unit.

Qgl **Glaciolacustrine deposits (Pleistocene)**—Silt and sand with subordinate clay and rare diamicton; compact and firm; light to medium gray or tan, locally slightly bluish where found at low elevations (below about 1,000 ft); typically thinly planar bedded to laminated, locally with rhythmic interbeds of sandy silt and silty clay; contorted beds are found locally where the unit is overlain by unit Qgd; springs and seeps are common at the top of this unit. Upstream from Twin Falls on the South Fork, unit Qgl is poorly exposed and appears to be laterally equivalent to the embankment deposit (unit Qgd) at the river canyon's mouth; where exposed, the deposits are somewhat less firm, sandier, and more tan than exposures along the Middle Fork. Along the Middle Fork at Mine Creek, this unit is exposed at the base of unit Qgd—and discontinuously upriver—and may correlate with and (or) underlie thick lacustrine deposits farther upriver outside the map area (Booth, 1990). The deposits of unit Qgl along the Middle Fork in the map area are more firm, less sandy, and slightly bluish compared to deposits along the South Fork. Together with the elevation and presence of overlying unit Qgd, these deposits likely formed during initial ice incursion before the establishment of the canyon-mouth embankments, whereas the deposits along the South Fork were more likely formed during glacial maximum after establishment of the embankments.

Fairhall and others (1966) obtained a 13,570 ^{14}C yr BP radiocarbon date on charcoal in lacustrine sediment—most likely from an exposure where the Grouse Ridge Road crosses the river (age site GD12). Porter (1976) and Booth (1986) interpreted this

age as indicative of deep lakes impounded by the Puget Lobe glacier, an interpretation with which we agree. A nearby radiocarbon date on charcoal from within thinly bedded sand and silt just below a sandy to pebbly diamicton lens (age site GD11) of 9,140 ^{14}C yr BP seems far too young to be related to glacial lakes; we suspect that the diamicton and immediately underlying layer may be a younger debris flow inset into the bedded deposits.

DEPOSITS OLDER THAN THE FRASER GLACIATION

Qad **Drift, alpine (Pleistocene)**—Unsorted mixture of boulders to pebbles in a matrix of coarse sand to clay; tan to brown, but locally somewhat gray; typically compact; grains and clasts are typically subrounded but range from angular to rounded; clasts are locally faceted and lithologies are representative of up-slope and (or) up-valley geology. The unit is mapped in upland areas, in alpine cirques, and along the valley walls of the Cedar River drainage. Although there are few good exposures of this unit owing to dense forest cover and thick soil, its geomorphic expression is clear in lidar: smooth except for slightly rumpled or dimpled surfaces, valley-margin-parallel ridges and crests (lateral moraines), cirque lakes, and locally prominent terminal moraines. The higher elevation of this unit distinguishes it from geomorphically similar (but lower) deposits of unit Qgic. As mapped, this unit contains some small deposits of colluvium and talus. Thickness of this unit is not well known, and likely varies substantially from a relatively thin veneer covering glacially scoured bedrock to more than 100-m thick in lateral moraines along valley walls.

We did not find clear evidence of alpine glaciers interacting with ice from the Puget Lobe, and regional work indicates that the alpine glaciation preceded the Puget Lobe by several thousand years (Porter, 1976). However, scattered remnants of poorly exposed drift on the valley wall directly north of Chester Morse Lake could plausibly have been deposited by either alpine glaciers (perhaps near their down-valley termini) or a narrow ice tongue of the Puget Lobe (near its up-valley extent). In this valley, clast lithologies of alpine and continental glacial deposits are quite similar and make distinguishing between the two difficult on this basis alone. Booth (1986) contends that ice of the Puget Lobe was grounded near the embankment deposits (unit Qgd on this map) at valley mouths, but likely extended farther upstream. It is thus possible that glacial deposits up to 6–10 km from the mouth of the Cedar River Valley could in fact be related to the Puget Lobe instead of local glaciers. This hypothesis is somewhat supported by the elevation of the deposits, which is similar to that for Puget Lobe lodgement till (unit Qgt) elsewhere in the map area.

Qguc **Glacial and nonglacial deposits, undivided (Pleistocene)**—Compact clay, silt, sand, minor gravel, and rare pebble to cobble diamicton; sand and silt are tan to light gray; clayey beds are gray to slightly blue; weathering of clasts and grains, where observed in coarser deposits, varies from moderate to strong and is overall greater than in deposits we consider to be younger; typically well consolidated to compact; silty or clayey beds commonly alternate with beds of fine to medium sand; thin to medium planar bedding is typical; thick beds of clay are uncommon; lithology of sand and gravel varies and could be locally derived; charcoal is locally present in more-extensive sandy deposits.

This unit is typically found beneath units Qgt, Qgic, or Qgd, and presumably rests directly on bedrock, though we found few such exposures; springs and seeps are common at the top of this unit. At least 70 m of nearly horizontal section is found near Twin Falls (base at ~700 ft elevation); Porter (1976) reports compact silt and clay at ~1,000 ft elevation that was uncovered (and re-covered) during interstate construction. This observation increases the thickness to ~100 m in this area. At least 45 m of dipping section is exposed along the South Fork east of Tanner butte; near river level, dips range from ~30 to 55 degrees northeast but steepen and are locally overturned near the top of the exposure where the unit is capped by several meters of compact till (unit Qgt). There are abundant small faults throughout the exposure and most have a northwest strike; offset on any strand is generally only a few centimeters, though some areas lack marker beds. We did not observe faults within the capping till layer in the field or on lidar. Faults are noted in most other exposures of unit Qguc and are discussed further in the *Evidence for Quaternary Faulting* section. The age of this unit is constrained by its stratigraphic position beneath till and four luminescence ages (age sites GD3, 4, 6, and 7), which indicate deposition prior to ~20 ka; the unit likely includes advance deposits of the Vashon Stade and deposits of the Olympia non-glacial period.

Tertiary Intrusive, Volcanic, and Sedimentary Rocks

The map area contains a remnant of middle Eocene sandstone and conglomerate beneath a latest Eocene through Oligocene intermediate to silicic volcanic succession. Cretaceous to Jurassic rocks of the western mélange belt underlie the Tertiary rocks, though we are uncertain if the contact is depositional or faulted where best exposed along the northwest flank of Mount Washington. Here the contact is generally(?) concordant with dips in unit ΦEv, but in some locations unit ΦEv appears to strike into the

underlying bedrock, suggesting some amount of buttressing. The contact is also locally faulted and (or) intruded by dikes and sills. Although we do not completely understand these relationships, we interpret the contact as a low-relief depositional surface with possibly some northwestward onlap.

Low-grade zeolitic alteration of the volcanic succession occurred shortly after burial (Hammond, 1963). Oligocene to Miocene mafic to felsic dikes and plutons intrude these altered rocks and are accompanied by an aureole of thermal metamorphism that locally extends 1 kilometer or more from the main intrusion. In general, this second alteration event is characterized by recrystallization with grain-size reduction, and ranges from pyroxene hornfels nearest the intrusion to epidote hornfels farther away. However, even where the original texture is not well preserved, it is usually possible to distinguish the presence of volcanic clasts, thus allowing for the gross distinction between flow rock and lapilli tuff or tuff breccia. The hornfelsed rocks are typically fine grained, very hard, and blue, blue-gray, or blue-green; where metamorphism is less pronounced, clasts in lapilli tuff or tuff breccia are multicolored. Most of unit OEv north of Chester Morse Lake is hornfelsed.

Migd **Granodiorite (Miocene)**—Medium-grained equigranular to slightly porphyritic granodiorite and minor diorite; white to light gray; jointing is common; lacks flow foliation; according to Erikson (1969) this is the Snoqualmie Granodiorite of Smith and Calkins (1906) and contains about 25 percent quartz, 10 percent orthoclase, 48 percent plagioclase, 9 percent hornblende, and 8 percent biotite, with trace augite and accessory minerals; however we note that mafic minerals are sparse in the map area. Compared to unit MOii or unit Ji_W, this unit lacks notable chloritic alteration. This unit intrudes rocks of unit $KJmm_W$ and unit $KJma_W$ west of Mailbox Peak, and Erikson (1969) notes that it locally intrudes the more-mafic phases of the batholith with clear cross-cutting relationships. Our boundary between this unit and the older diorite (unit MOii) is placed farther west than that of Erikson (1969) or Tabor and others (2000) because we find gabbro near the Fire Training Center along Grouse Ridge Road (geochemical site G1 and age site GD5). In the map area, the age of unit Migd is constrained by its intrusive relationship with unit MOii. Plagioclase from age site GD5 (unit MOii) yields an age of 21.01 ±0.10 Ma, much younger than the ~25 Ma ages on biotite and groundmass from the same sample. We suspect that intrusion of unit Migd may have locally reheated age site GD5 (which is at most a few hundred meters away) and if so, helps limit the age of unit Migd to sometime after ~21 Ma. Tabor and others (2000) report several K-Ar ages on biotite from rocks they map as granodiorite of the Snoqualmie batholith; these range from ~17–20 Ma.

MOii **Intermediate intrusive rocks (Miocene to Oligocene)**—Medium- to fine-grained diorite, gabbro, monzonite, and minor granodiorite to tonalite; light to medium gray, typically with a slight greenish hue; mostly equigranular, locally porphyritic; jointing is locally prominent and parallels the intrusive contact. Erikson (1969) reports that these rocks in the vicinity of the South Fork are olivine-bearing (up to a few percent) and largely composed of calcic plagioclase, varying amounts of hypersthene and augite, and minor biotite with trace hornblende; our work confirms these general trends, though in areas farther south we did not find olivine but instead found locally abundant opaque minerals. Most rocks show some amount of alteration, including varying levels of chloritic replacement of mafic minerals and sericite replacement of feldspars. In at least one location (thin-section site TS28) we noted a granoblastic texture, indicating recrystallization and grain-size reduction due to younger intrusions. Perhaps this is the granodiorite of the Snoqualmie batholith mapped just east of that location by Tabor and others (2000). No ductile shearing of these rocks was noted in the field or in thin sections, in contrast to some rocks of unit Ji_W. However, where the Mesozoic rocks lack such shearing, they are nearly indistinguishable from the gabbro and diorite of this unit.

The small but numerous outcrops of this unit in the southeastern part of the map area—in combination with hornfelsing of volcanic rocks here—suggests that the intrusive rocks we see at the surface are apophyses of a much-larger intrusion (or intrusions) beneath the surface. The age of this unit is based on its intrusive relationship with rocks of unit OEv throughout the map area and a $^{40}Ar/^{39}Ar$ age on biotite in gabbro of 24.8 Ma (age site GD5; geochemical site G1). Our date of ~153 Ma on gabbro mapped by Erikson (1969) as a border phase of the Miocene Snoqualmie batholith (age site GD13) supports the contention of Tabor and others (2000) that at least some of the more-altered rocks in that area are Jurassic instead of Tertiary, and suggests that Jurassic-age intrusive rocks might be even more prevalent than currently mapped.

MOir **Rhyolite, intrusive (Miocene to Oligocene)**—Fine-grained rhyolite; maroon, pink, lavender, or gray; well indurated; sparsely porphyritic with an aphanitic to cryptocrystalline groundmass and 1–2 mm plagioclase phenocrysts with uncommon phenocrysts of irregular 0.5–2 mm quartz; laths of plagioclase microlites in the groundmass are slightly trachytic. Near-vertical flow foliation and banding is prominent, distinctive, and divides the rock into 1–5-cm-thick plates. Unit is mapped only northwest of Rack Creek where outcrop pattern and dip of foliation indicate that it intrudes rocks of unit OEv and may intrude rocks as young as unit Ovt; thickness is difficult to constrain but ranges from 10–120 m perpendicular to the flow foliation. Our

age of 25.6 Ma on a prominent tuff near exposures of unit ᏔᎾir (age site GD20) is about 4–5 million years too young based on its stratigraphic position beneath unit ᎾEvt; this out-of-sequence age may be the result of reheating during intrusion of units ᏔᎾir and (or) ᏔᎾib.

ᏔᎾib **Basalt dikes and sills (Miocene to Oligocene)**—Aphanitic to very sparsely plagioclase-phyric basalt dikes; black to very dark gray; weathers gray to brown; well indurated; locally splintery to hackly; generally lacks flow foliation; 0.5 to 2 m or more in width with fine-grained to aphanitic margins; dikes wider than about 1 m typically have crude margin-perpendicular fractures or, more rarely, sub-horizontal columns; vesicles are absent except locally at some dike margins. Unit is sparsely mapped south of Interstate 90 and is likely more prevalent than indicated. The rock of this unit is the least altered of any observed in the map area; it cuts all types of extrusive volcanic rocks and cuts unit $KJma_W$ downstream of Twin Falls on the South Fork; no exposures were found near other types of intrusive rock. The age of this unit is inferred from lack of alteration and cross-cutting relationships.

ᎾEvt **Tuff (Oligocene)**—Crystal-vitric lapilli tuff; light green to greenish white; somewhat friable, poorly welded to unwelded; most clasts are lapilli size and subrounded to subangular; cobble-sized clasts are ubiquitous but rarely abundant; matrix of greenish ash, with both fragments and euhedral laths of plagioclase phenocrysts (0.5–3 mm) and minor pyroxene and quartz; flattened pumice fragments are not abundant. Petrographic analysis (thin section TS34) reveals locally prominent flow banding where matrix material is compressed against the edges of grains and clasts (including clasts of black to dark brown vitrophyre). This unit is only mapped in the far southwestern corner of the map where it forms a bold outcrop that can be traced westward; the outcrop pattern and dips indicate a thickness of ~50–70 m. This unit was mapped by Hammond (1963) as the Tuff of Stampede Pass, which he regarded as a regionally extensive deposit sourced from vents southeast of Snoqualmie Pass. Tabor and others (2000) included these rocks in their dacitic Tuff member of Lake Keechelus. Multiple ages from this unit are reported in Tabor and others (1984), Dragovich and others (2009a), and Hammond and Dragovich (2008) and span a few million years in the Oligocene: K–Ar and $^{40}Ar/^{39}Ar$ ages range from 28.2–29.9 Ma, three zircon grains yield U-Pb ages of ~29–31 Ma, and a zircon fission-track age of 30.4 Ma is from near the source area of these rocks to the east. The reason for the age dispersion is not entirely clear, but a flow within the tuff (outside of the current map area) could indicate that it is a composite unit instead of a single eruptive event, as noted by Hammond (1963).

ᎾEiv **Intrusive dikes and sills (Oligocene to Eocene)**—Aphanitic to porphyritic basalt, andesite, and possibly dacite to rhyolite; gray to tan where fresh, all with various shades of green to blue; locally altered (or weathered) brown, red, or orange; commonly well indurated; locally silicified, most commonly near faults. Unit contains 1–3-mm grains of sparse to abundant plagioclase that are commonly altered to sericite, clay, and (or) calcite, and minor amounts of tabular pyroxene that is typically partially altered to chlorite; locally trachytic with euhedral, nearly acicular plagioclase. Found as 1–2-m-wide dikes and sills within unit ᎾEv where their similarity to flows of unit ᎾEv makes differentiation from the flows difficult; as such, dikes and sills are likely more prevalent than mapped. Faults are common along dike edges, but it is not clear if these formed during emplacement or after, and the amount of displacement is probably less than a few meters. A dike and sill intrude units Ji_W and $KJma_W$ on the northwest flank of Mount Washington (along the Olallie trail) just below the base of unit ᎾEv; these may represent a portion of the plumbing system for the overlying Oligocene to Eocene volcanic rocks. The age of this unit is constrained by its lithologic similarity with flows of unit ᎾEv and their similar degree of alteration; unit ᎾEiv differs in these traits from rocks of unit ᏔᎾib.

ᎾEvc **Volcaniclastic rocks (Oligocene to Eocene)**—Tuffaceous siltstone, pebbly diamictite, and interbedded coarse sandstone; gray, tan, and light green where fresh; weathers brown to dark gray; moderately indurated to fissile; siltstone beds are 10–20 cm thick and are finely bedded to laminated; sandstone beds are of similar thickness, about half as prevalent as the siltstone, moderately sorted, and thinly to thickly planar bedded; grains are mostly subrounded, range from coarse sand to granule, and appear to be predominantly sourced from volcanic rock. The pebbly diamictite has an ashy to silty matrix and the well-distributed clasts are all volcanic; we interpret the diamictite as distal lahar deposits or debris flows. This unit is only mapped below unit ᎾEvt northwest of Rack Creek where a 10-m-thick section is exposed; contacts with unit ᎾEv were not found. A lithologically similar unit is mapped in greater abundance and thickness west and south of here by Hammond (1963). Combined with the general lack of good exposure in this area, this leads us to suspect that unit ᎾEv is probably more prevalent than currently shown.

ᎾEv **Volcanic rocks, flows, and tuffs (Oligocene to Eocene)**—Dark gray, black, or blue aphanitic to

porphyritic flows with varying amounts of plagioclase, hornblende, and pyroxene; flows are 1–5 m thick, rarely vesicular, typically somewhat recrystallized, and more prevalent in the middle of the unit. Tan, blue, or grayish green tuff, lapilli tuff, and tuff breccia with varying proportions of crystal, lithic, and vitric components comprise most of the lower and upper portions of the unit; crystal-vitric lapilli tuff is most common; clasts within tuffs are predominantly aphanitic to porphyritic volcanic rock; pumice clasts are common, locally abundant, and typically partially welded; non-volcanic clasts are almost entirely absent, though Tabor and others (2000) note sparse clasts of mélange-belt rock. Bed thickness ranges from a few meters to >50 m. We estimate a range of unit thicknesses from the map and cross sections: about 1,600 m lies beneath unit ΦEvt south of Chester Morse Lake; north of the lake we estimate ~1,300–1,800 m. Notably, we estimate about 650 m beneath the 34.5 Ma age at site GD16, but only ~350 m beneath a similar age (34.7 Ma) at site GD10. Northwestward onlap, as we show in the cross sections, could account for the difference, as could faulting. Our estimates are lower than those of Hammond (1963) and Fuller (1925) in this area, but they defined their units differently.

Geochemically, the unit ranges from basaltic andesite to dacitic rhyolite (geochemical sites G2 and G4–G8). Rocks of unit ΦEv are typically altered to at least zeolite facies and are locally also hornfelsed near intrusions; both types of alteration make field identification of protolith difficult. Ages range from 34.7 to 18.4 Ma (age sites GD9–10, GD14, and GD16–20), though we believe that many (or most?) of the $^{40}Ar/^{39}Ar$ ages are too young, likely the result of reheating because the unit is locally adjacent to intrusive rocks.

This unit forms the prominent ridgeline south of Interstate 90; one outcrop north of the interstate is very hornfelsed and is mapped with a depositional contact on unit Jiw, though there are also small dioritic intrusions that cut the altered lapilli tuff and are presumably related to the Snoqualmie batholith. Rocks of this unit were mapped by Tabor and others (2000) as part of the Ohanapecosh Formation, and by Hammond (1963) as the flow-dominated Enumclaw Formation and overlying tuffaceous Huckleberry Mountain Formation.

Ecg **Conglomerate and sandstone (late to middle Eocene)**—Pebble conglomerate with interbeds and lenses of lithic to arkosic and micaceous medium sandstone to pebbly sandstone; gray to tan where fresh, weathering brown and orange; sandy beds are well sorted and grain supported; pebbles and rare, small cobbles are typically subrounded, whereas smaller clasts and grains are more commonly subangular; conglomerate is moderately to poorly sorted, with up to 10 percent gray to tan ashy mud matrix; unit typically lacks distinctive stratification, but crude planar(?) stratification is found locally in coarser beds and a 4–5-cm-thick interval of low-angle cross stratification is found in a sandy bed. Individual bed thickness is difficult to constrain, but bedding-parallel ridges tend to be conglomerate beds and appear to be 1–10 m thick; sandstone beds are probably at least equal to or thicker than the conglomerate beds, although they do not generally crop out; overall unit thickness is likewise difficult to constrain as neither the bottom nor top of the unit are observed; based on map extent and bedding dip, we estimate at most a few hundred meters where the unit is best constrained: low on the western ridge leading to Mount Washington, where it was first noted by Foster (1955). Clasts are unique for the map area and include abundant and resistant dark gray to black chert or quartzite with white veins, slightly less abundant light gray, tan, and light green tuffaceous clasts (which are more angular than dark-colored clasts), a few fine-grained granitic clasts, and sparse but distinctive red jasper. The base of the unit contains a poorly exposed vesicular and trachytic andesite flow (thin-section site TS19) that is probably a few meters thick and appears to lie on unit Jiw.

We interpret detrital U-Pb ages (age site GD15) to indicate deposition after ~47 Ma. Of the 112 ages, 75 are Late Jurassic, which combined with the abundance of chert, suggest rocks of the eastern mélange belt may be a source, as interpreted by Tabor and others (2000). Unit Ecg could correlate to the Raging River or Tiger Mountain Formations to the west, which have a similar stratigraphic position, a similar suite of conglomerate clast lithologies, and westward paleocurrents (Vine, 1969; Johnson and O'Connor, 1994). Alternatively, or in addition, this unit could correlate with the Guye Sedimentary Member of the Naches Formation of Tabor and others (2000) to the east, as originally proposed by Hammond (1963). Although Tabor and others (2000) considered the base of the Naches Formation to be younger than these rocks, a 49.7 Ma age from the Mount Catherine Tuff Member (Eddy and others, 2016) is permissive of a correlation.

Mesozoic Low- and Medium-Grade Metamorphic Rocks of the Western Mélange Belt

The oldest rocks in the map area are Cretaceous to Jurassic marine metasediments, metavolcanics, and meta-intrusives that are mapped as part of the western mélange belt (WMB) by Tabor and others (2000). Recent mapping north of here suggests that the mélange belt may be composed of a lower and upper sheet of metasedimentary and metavolcanic rock separated by a middle sheet of meta-intrusive rock (Dragovich and others, 2014). Although we lack sufficient exposure to test the hypothesis, it

can explain the distribution of lithologies in the map area. Near the contact between unit Ji_W and $KJmv_W$ south of Mount Si, there are some brittle-ductile fault rocks that contain altered pseudotachylyte (thin section site TS4), and a thick package of very deformed meta-gabbro and minor amphibolite is west of Mount Washington and near the contact with unit $KJms_W$; both of these areas are near major thrusts in the model of Dragovich and others (2014), though sheared and altered rocks are prevalent in many exposures of WMB rocks. In thin section, chlorite, epidote, calcite, and quartz are common secondary minerals, and in combination with locally developed foliation, indicate metamorphism near greenschist facies as described in detail by Tabor and others (1993; 2000).

Along the corridor of the Middle Fork, foliation and bedding in these rocks dips moderately to steeply southeast, even adjacent to the steep intrusive contact with unit Migd. South and west of here the rocks generally dip moderately to steeply west–southwest and locally show well-developed small-scale folds with northwest axes. West dips are uncommon throughout the WMB (Tabor and others, 2000) and these may define a broad north–northwest-trending antiform through the center of the map area, though it is too speculative to place on the map.

$KJmm_W$ **Marine metasedimentary rocks, undivided (Cretaceous to Jurassic)**—Fine sandstone, argillite, and minor chert; dark blue, black, off-white, or tan; composed of any of the sedimentary facies described below. Also includes a section on Mailbox Peak of thin, rhythmically interbedded medium-blue sandstone and siltstone with off-white chert(?). The unit is mapped where the proportion of sandstone and argillite are either difficult to determine or vary. The northwest flank of Mailbox Peak is a nearly continuous dip panel of this unit, which is 2,250–2,400 m thick based on dips and outcrop extent. The map pattern indicates that there is a steep cut-off angle between these rocks and intrusive rock of the Snoqualmie batholith (units Migd and MOii). Where exposures of dark blue to dark gray fine-grained sandstone lack interbeds of argillite or conglomerate, it is difficult to distinguish this unit from the dark blue to gray metavolcanic rock of unit $KJmv_W$ and the dark-colored altered aphanitic flows of unit OEv; the presence of angular sand grains is distinctive, but not always identifiable in the field. This problem is particularly acute where rocks have been thermally altered (and locally recrystallized) by intrusion of the Snoqualmie batholith. Unit $KJmm_W$ is locally subdivided into:

$KJma_W$ **Argillite-rich facies**—Argillite with subordinate shale, phyllite, slate, and fine sandstone; dark blue to black; generally lacks well-preserved sedimentary structures, but is locally finely laminated to thinly bedded. Most exposures show a penetrative metamorphic fabric that ranges from weakly developed cleavage to well-developed foliation; where phyllitic or slatey, acutely intersecting cleavage planes are common and divide the rock into lenses, pods, and phacoids that range from millimeters to several meters in width; commonly contains abundant disrupted millimeter- to centimeter-wide white veins of calcite, quartz, and albite(?). This unit was mapped expansively by Tabor and others (2000), but we restrict its usage to outcrops in which sandstone and other lithologies are subordinate to argillite.

$KJms_W$ **Sandstone-rich facies**—Fine-grained sandstone with subordinate argillite and chert, and minor conglomerate; dark gray to dark blue; sandstone ranges from very fine to medium grained and is typical in medium to thick beds separated by thin to medium beds of contorted or disrupted argillite; sand grains are mostly angular to subrounded in thin section, but commonly too small to see well in hand sample; polycrystalline quartz grains are typically rounded and are likely chert. Conglomerate is found locally near Mine Creek along the Middle Fork and upstream of Twin Falls on the South Fork and is composed of elongate, subrounded to rounded granules to small pebbles, mostly of chert, in a sandy matrix; shale rip-up clasts are locally preserved. In general, sandstone appears somewhat recrystallized but lacks visible metamorphic foliation, in contrast to the slaty to foliated argillite and the elongate (stretched) pebbles in the conglomerate. Veins are locally abundant, mutually offset each other, and range from a few millimeters to several centimeters wide. We interpret a detrital zircon sample (age site GD8) from a thick sandstone bed bracketed by argillite in the riverbed downstream of Twin Falls as indicating deposition after ~86.5 Ma. Of the 108 grain ages, almost half are Cretaceous, nearly half are Jurassic, and there are a few Triassic to pre-Cambrian ages.

$KJmc_W$ **Chert-rich facies**—Rhythmic thin to thick beds of tan to off-white chert interbedded with subordinate thin to medium beds of medium gray to black argillite and minor fine- to very-fine-grained dark blue to gray sandstone; very indurated. Best exposed in and near the narrow bedrock gorge on the South Fork; here and in an exposure just below the interstate there are abundant, nearly isoclinal folds with gentle northwest and southeast plunges and 1–2

m wavelengths. An additional exposure of chert is found near the trail bridge above Twin Falls.

$KJmv_W$ **Greenstone (Cretaceous to Jurassic)**—Aphanitic to rarely porphyritic rock; dark gray, black, dark blue, or dark green; generally somewhat sheared; lacks any distinctive igneous or sedimentary structures; typically found as large blocks and pods in a scaly argillite matrix; disseminated pyrite is common; hematite-coated fractures and small faults are also common; the nearly ubiquitous veins seen in other rocks of the WMB seem far less abundant in this unit, though it is only sparsely mapped compared to the other units.

Ji_W **Meta-intrusive rocks (Jurassic)**—Altered gabbro and diorite, subordinate tonalite, and minor amphibolite; typically light gray to salt-and-pepper in appearance, and usually has a greenish cast; generally equigranular to slightly porphyritic; medium grained, but locally varies from fine to coarse. Deformation and alteration in these rocks range from alteration of mafic minerals to chlorite without any shearing through incipient foliation and development of local, thin, ductile shear zones; metamorphic minerals generally indicate sub-greenschist facies and include chlorite, epidote, and calcite, with locally abundant opaque minerals; one sample northwest of Mount Washington (thin-section site TS16) had glaucophane filling a thin vein and suggests that sub-blueschist facies may have existed at least locally. Rocks of this unit mapped south of the South Fork also have a nearly penetrative cataclastic deformation imprinted on the ductile fabric; this is not observed in other rocks of the western mélange belt in this map area, but the reason for the brittle deformation is not entirely clear; a series of low-angle faults (thrusts?) cut this section, but where they are best exposed (at low elevation), there is relatively little brittle deformation.

We generally use the presence of alteration and deformation to distinguish these older intrusive rocks from Oligocene to Miocene intrusive rocks. Our age at site GD13 near the eastern edge of this map confirms the interpretation of Tabor and others (2000) that some portion of the gabbro in this area is Jurassic and not a border phase of the Snoqualmie batholith, as proposed by Erikson (1969). The similarity in both hand sample and thin section between some Jurassic gabbro and other nearby exposures of gabbro and diorite suggests that there could be more Jurassic-age rock than is currently mapped. Zircons from two medium-grained sites with relatively little alteration (age sites GD2 and GD13) yield concordia ages of 155.79 ±0.35 Ma and 152.97 ±0.34 Ma, which we interpret as their crystallization age. Geochemical analysis collocated with age site GD13 (geochemical site G3) and thin sections (sites TS3, 4, 9, and 16) indicate the rock is gabbro.

EVIDENCE FOR QUATERNARY FAULTING

We do not find any evidence for deformation of Vashon-age or younger deposits, and none of our observations require us to infer such deformation. However, many exposures of pre-Vashon deposits (unit Qguc) are tilted and (or) faulted. West of Tanner butte along the South Fork, a well-exposed section of unit Qguc dips moderately to steeply northeast, is locally overturned, has numerous steep to moderately dipping north–northwest-striking faults of varying slip sense, and appears to be capped by at least 1.5 m of horizontal till. A luminescence age (age site GD4) from near the base of the faulted section and the presence of a seemingly undisturbed till at the top of the cliff indicate that deformation occurred between 15 ka and ~40 ka. Unit Qguc is also clearly faulted in a steep road cut near Derry Lake at age site GD6 (42 ka) where steeply dipping north–northwest-striking faults have mostly west-down offset. A thrust fault displacing pre-Vashon sediment was noted by Porter (1976) during construction of Interstate 90 above Twin Falls at ~1,000 ft elevation, though the outcrop no longer exists and the direction of movement was not described. Nearby and at slightly lower elevation (885 ft), we find horizontally bedded pre-Vashon sediment in natural exposures along the trail to Twin Falls, and date one such exposure to 49 ka (age site GD7).

Both bedrock and a poorly exposed outcrop of unit Qguc are faulted near the outcrop of unit Ji_W on Boxley Creek. We infer and place a fault just northeast of the bedrock in Boxley Creek to honor the fault observations in both bedrock and younger deposits. We refine the strike and slip sense of the fault by using observations of the bedrock-sediment contact in the northwest quadrant of the map area, as constrained by sparse bedrock outcrops and by assessing the depth to bedrock from more abundant water-well records (water wells W8–13, 15–23, 25–36). These can be interpreted to indicate a north–northwest-trending northeast-down drop of ~50 m over a horizontal distance of as little as 170 m along the fault crossing Boxley Creek. Though this seems to support our contention of a fault in this location, the depth-to-bedrock data as a whole indicate an overall northeast dip to the bedrock contact and suggest many tens of meters of paleotopography. Thus it is also possible to view the ~50 m drop as paleotopography without any faulting, though we prefer the fault interpretation because of the narrow width of the change in elevation and its coincidence with faulted bedrock and younger deposits.

It is difficult to interpret the numerous exposures of faulted pre-Vashon deposits and two main hypotheses compete. In the first, the Puget Lobe glacier scoured and deformed the existing pre-Vashon sedimentary deposits as it advanced into the region, in some places removing them completely and in other places tilting and shearing them; tectonic faulting is not required. The second hypothesis assumes that all the tilting and faulting we observe is related to movement along the numerous (mostly northwest-striking) tectonic faults that project into the map area, including strands of the Rattlesnake Mountain fault zone,

which Dragovich and others (2009a) interpret as active. The observation that only pre-Vashon deposits are deformed can be reconciled with either hypothesis: either it demonstrates that the deformation is related to the glacier, or that all the tectonic faulting is pre-Vashon. The northwest strike of the observed faults seems to fit better with a tectonic interpretation because there are other known northwest-striking active Quaternary faults nearby and because we expect deformation related to advancing glaciers to be perpendicular to ice advance, which in this case would predict northeast strikes. In contrast, the patchy distribution of pre-Vashon deposits strongly supports the idea that the glacier substantially altered the valley floor as it advanced. Together, no line of reasoning is more compelling than the others and we suspect that both glacial deformation and tectonic faulting have affected the region, though the proportion of each remains difficult to ascribe.

INTERPRETATION OF GEOPHYSICAL FEATURES

We combine our newly collected gravity data with existing gravity and aeromagnetic data to better understand the subsurface distribution of geologic units in the area (Fig. M1). Measurements of magnetic susceptibility and density for representative rock samples augment the map data. We explore correlations between the potential-field data and the mapped geology below.

Influence of the Snoqualmie Batholith

The strongest aeromagnetic high in the area (1,930 nT; HH in Fig. M1) fills the southeastern corner of the map and continues east and south. The extent and peak amplitude of this anomaly correlates with hornfelsed volcanic lithologies that surround the Snoqualmie batholith; the measured magnetic susceptibilities of the hornfelsed lithologies are extremely high (average χ = 37 x 10^{-3} SI; one outcrop averaged 75 x 10^{-3} SI). The extent of this magnetic high also broadly correlates with the mapped extent of diorite and gabbro (units Migd and MOii), though the intrusive rock is only moderately magnetic (average χ = 15 x 10^{-3} SI). A subtle gravity high (~5 mGal compared to surrounding regions) is associated with the magnetic anomaly and likely results from the slightly higher density of the diorite (average ρ = 2,710 kg/m^3 from samples and 2,735–2,845 kg/m^3 from modeling) and hornfelsed lithologies (ρ = 2,750 kg/m^3) compared to country rock (WMB average ρ = 2,730 kg/m^3) and non-hornfelsed volcanic rock of unit OEv (average ρ = 2,600 kg/m^3). Based on the correlation between high gravity and magnetic anomalies with the batholith and surrounding hornfelsed rocks, we believe that the batholith occupies much of the upper crust within the eastern half of the quadrangle. Cross section modeling supports this interpretation and also suggests that there may be three zones of the batholith under the map area: granodiorite (unit Migd) and two zones of diorite (unit MOii) that differ slightly in magnetism and density (Fig. M1). The edge of the batholith in our model is relatively well-determined at depth by the gravity, and a steep magnetic gradient (HG in Fig. M1) constrains the near-surface edge of strongly hornfelsed rocks adjacent to the batholith.

Influence of the Western Mélange Belt

Features of the western mélange belt (WMB) in the map area are less distinctive than those related to the Snoqualmie batholith. From a potential-field geophysics perspective, the WMB in this area is divided into: (1) metasediment with minor metavolcanic rock (units $KJmm_W$ and $KJmv_W$); and (2) meta-intrusive rock, predominantly gabbro (unit Ji_W). The density of the metasedimentary rock is slightly higher than average values for upper crustal rock and the metasediment generally lacks magnetism (Fig. M1). However, the metagabbro is both more dense and more magnetic than the metasedimentary rock and is correlated with subtle, relative aeromagnetic highs (~25 nT) and similarly subtle (3–4 mGal) gravity highs such as near Mount Si and Rattlesnake Lake (MGHs and MGHr, respectively, in Fig. M1). We use this correlation to infer the presence of metagabbro in other locations (such as MGH in Fig. M1) and include laterally-limited metagabbro on our cross section model, though the exact extent and shape are not well-constrained.

Major Structures

Although most gravity anomalies across the map area are small (5–6 mGal or less), a steep, south-facing gravity gradient (values decrease southward) begins in the southwest corner of the map area and culminates in a ~15 mGal relative gravity low (SL on Fig. M1) southwest of the quadrangle. This gravity low correlates with a large structural low known as the Green River syncline (Hammond, 1963), and indicates that it is filled with low-density material. Preliminary modeling indicates the strong gravity gradients on the edges of this gravity low arise from faults just off the quadrangle to the southwest. Linear aeromagnetic highs paralleling the gravity contours (VF on Fig. M1) appear to correlate with the volcanic rocks of Eagle Gorge of Tabor and others (2000) and may be particularly magnetic volcanic flows. The edge of the syncline is barely included in our cross-section model, but the multiple flow and tuff layers with differing magnetic properties filling the edge of the syncline are strongly supported by geologic mapping, measured rock properties, and the potential-field anomalies themselves.

A strong northwest-trending magnetic high (RFH on Fig. M1)—the edges of which are associated with main strands of the Rattlesnake Mountain fault zone (RMFZ; Dragovich and others, 2009a)—does not appear in the current map area. Northwest-trending gravity gradients are not strong (for example, RG on Fig. M1) and do not appear to cross the edge of the batholith. Despite this, both the mapped geology and the high-resolution gravity data along the cross section in our model strongly support a fault in this area, with offset imparting a change in the thickness of the volcanic rocks. This offset creates a narrow but strong step in the gravity (RG in Fig. M1). This strong step does not continue far to the northwest or southeast in map view, which we interpret as a lack of consistent dip-slip offset on the structure and perhaps more strike-slip than dip-slip offset. Based on its steep geometry at the surface and in the geophysical models, we suspect this fault may be a minor strand of the RMFZ.

We suspect there may be an additional northwest-striking fault south of the fault discussed above that follows the valley of the Rex River (Fig. M2). Under the southwestern edge of Chester

Morse Lake, an abrupt, short-wavelength change in gravity (PF in Fig. M1) could signify a fault. However, we lack both the geophysical and geologic data to interpret this anomaly with any confidence. If this structure exists, it might serve to link faults of the RMFZ with those we hypothesize forming the edges of the deep syncline to the south (SL in Fig. M1).

Other Features

A few features in our map and model are not well defined but are still worth noting. On the cross section model (Fig. M1) we do not precisely match several short-wavelength anomalies just northeast of Chester Morse Lake. These anomalies could be due to small unmapped faults in this region or due to individual flows within the volcanic succession. We prefer the latter interpretation because we know there are abundant flows in the map area that are too small to map. At the southwest end of the cross section model (Fig. M1), the intrusive rhyolite (unit MOir) has similar physical properties to average basement material and the overlying volcanic rock and is therefore not well constrained by potential fields. The nearby basaltic dike (unit MOib) does help explain both geologic map patterns and a short-wavelength (~500 m or less) gravity anomaly directly above its location (MD in Fig. M1). Finally, two of the most-prominent relative gravity lows are in the north–central part of the map area (GL in Fig. M1). We did not model these lows, but they correlate with thick (up to nearly 300 m) accumulations of subglacial deposits (unit Qgd), which should be of low-enough density to generate these gravity lows.

ACKNOWLEDGMENTS

We would like to thank the City of Seattle for providing access to the Cedar River Watershed. From WGS, Alison Horst provided two weeks of assistance with geologic mapping and Emilie Richard and Maria Furtney each provided one week; Alex Dolcimascolo provided two weeks of assistance with gravity data collection. Also from WGS, Michael Polenz and Andrew Sadowski provided initial review of the map and writing, and Maria Furtney, Dan Coe, and Susan Schnur provided review, editing, figure production, and layout; data stewardship was provided by Ashley Cabibbo. Mike Arnold of Dacite Environmental LLC provided helpful observations of geology along the Snoqualmie River and Olallie Trail in addition to insightful discussions on the geologic evolution of the map area.

AUTHOR CONTRIBUTIONS

The geologic mapping was completed by A. Steely, with assistance from K. Alexander, A. Horst, E. Richard, and M. Furtney. Gravity data was collected by M. Anderson with assistance from K. Alexander and A. Dolcimascolo. Geologic analysis was completed by A. Steely; Cross Section A was completed by K. Alexander, and the corresponding geophysical model was completed by M. Anderson; Cross Section B was completed by K. Alexander and A. Steely. The writing was led by A. Steely, with additions from M. Anderson.

REFERENCES

Barnes, D. F.; Oliver, H. W.; Robbins, S. L., 1969, Standardization of gravimeter calibrations in the geological survey: Eos, Transactions American Geophysical Union, v. 50, no. 10, p. 626–627. [https://doi.org/10.1029/EO050i010p00526]

Black, L. P.; Kamo, S. L.; Allen, C. M.; Davis, D. W.; Aleinikoff, J. N.; Valley, J. W.; Mundil, R.; Campbell, I. H.; Korsch, R. J.; Williams, I. S.; Foudoulis, Chris, 2004, Improved $^{206}Pb/^{238}U$ microprobe geochronology by the monitoring of a trace-element-related matrix effect; SHRIMP, ID-TIMS, ELA-ICP-MS and oxygen isotope documentation for a series of zircon standards: Chemical Geology, v. 205, no. 1–2, p. 115–140. [https://doi.org/10.1016/j.chemgeo.2004.01.003]

Blakely, R. J.; Wells, R. E.; Weaver, C. S., 1999, Puget Sound aeromagnetic maps and data: U.S. Geological Survey Open-File Report 99-514, version 1.0. [https://pubs.er.usgs.gov/publication/ofr99514]

Blakely, R. J.; Sherrod, B. L.; Weaver, C. S.; Wells, R. E.; Rohay, A. C.; Barnett, E. A.; Knepprath, N. E., 2011, Connecting the Yakima fold and thrust belt to active faults in the Puget Lowland, Washington: Journal of Geophysical Research, v. 116, no. B7, 33 p. [https://doi.org/10.1029/2010JB008091]

Booth, D. B., 1986, The formation of ice-marginal embankments into ice-dammed lakes in the eastern Puget Lowland, Washington, U.S.A., during the late Pleistocene: Boreas, v. 15, no. 3, p. 209–264. [https://doi.org/10.1111/j.1502-3885.1986.tb00929.x]

Booth, D. B., 1990, Surficial geologic map of the Skykomish and Snoqualmie Rivers area, Snohomish and King Counties, Washington: U.S. Geological Survey Miscellaneous Investigation Series Map I-1745, 1 sheet, scale 1:50,000. [https://doi.org/10.3133/i1745]

Booth, D. B., 1994, Glaciofluvial infilling and scour of the Puget Lowland, Washington, during ice-sheet glaciation: Geology, v. 22, no. 8, p. 695–698. [https://doi.org/10.1130/0091-7613(1994)022<0695:GIASOT>2.3.CO;2]

Booth, D. B.; Goldstein, B. S., 1994, Patterns and processes of landscape development by the Puget Lobe ice sheet. *In* Lasmanis, Raymond; Cheney, E. S., convenors, Regional geology of Washington State: Washington Division of Geology and Earth Resources Bulletin 80, p. 207–218. [https://www.dnr.wa.gov/publications/ger_b80_regional_geol_wa_1.pdf]

Bretz, J H., 1913, Glaciation of the Puget Sound region: Washington Geological Survey Bulletin 8, 244 p., 3 plates.

Brocher, T. M.; Blakely, R. J.; Wells, R. E., 2004, Interpretation of the Seattle uplift, Washington, as a passive-roof duplex: Bulletin of the Seismological Society of America, v. 94, no. 4, p. 1379–1401. [https://doi.org/10.1785/012003190]

Chang, Zhaoshan; Vervoort, J. D.; McClelland, W. C.; Knaack, Charles, 2006, U-Pb dating of zircon by LA-ICP-MS: Geochemistry, Geophysics, Geosystems, v. 7, no. 5, 14 p. [https://doi.org/10.1029/2005GC001100]

Crandell, D. R., 1963, Surficial geology and geomorphology of the Lake Tapps quadrangle, Washington: U.S. Geological Survey Professional Paper 388-A, 2 plates, scale 1:24,000, with 84 p. text. [https://doi.org/10.3133/pp388A]

Dragovich, J. D.; Anderson, M. L.; Walsh, T. J.; Johnson, B. L.; Adams, T. L., 2007, Geologic map of the Fall City 7.5-minute quadrangle, King County, Washington: Washington Division of Geology and Earth Resources Geologic Map GM-67, 1 sheet, scale 1:24,000. [https://www.dnr.wa.gov/publications/ger_gm67_geol_map_fallcity_24k.zip]

Dragovich, J. D.; Walsh, T. J.; Anderson, M. L.; Hartog, Renate; DuFrane, S. A.; Vervoot, Jeff; Williams, S. A.; Cakir, Recep; Stanton, K. D.; Wolff, F. E.; Norman, D. K.; Czajkowski, J. L., 2009a, Geologic map of the North Bend 7.5-minute quadrangle, King County, Washington, with a discussion of major faults, folds, and basins in the map area: Washington Division of Geology and Earth Resources Geologic Map GM-73, 1 sheet, scale 1:24,000. [https://www.dnr.wa.gov/Publications/ger_gm73_geol_map_northbend_24k.zip]

Dragovich, J. D.; Littke, H. A.; Anderson, M. L.; Hartog, Renate; Wessel, G. R.; DuFrane, S. A.; Walsh, T. J.; MacDonald, J. H., Jr.; Mangano, J. F.; Cakir, Recep, 2009b, Geologic map of the Snoqualmie 7.5-minute quadrangle, King County, Washington: Washington Division of Geology and Earth Resources Geologic Map GM-75, 2 sheets, scale 1:24,000. [https://www.dnr.wa.gov/Publications/ger_gm75_geol_map_snoqualmie_24k.zip]

Dragovich, J. D.; Littke, H. A.; Anderson, M. L.; Wessel, G. R.; Koger, C. J.; Saltonstall, J. H.; MacDonald, J. H., Jr.; Mahan, S. A.; DuFrane, S. A., 2010, Geologic map of the Carnation 7.5-minute quadrangle, King County, Washington: Washington Division of Geology and Earth Resources Open File Report 2010-1, 1 sheet, scale 1:24,000, 21 p. text. [https://www.dnr.wa.gov/Publications/ger_ofr2010-1_geol_map_carnation_24k.zip]

Dragovich, J. D.; Anderson, M. L.; Mahan, S. A.; MacDonald, J. H., Jr.; McCabe, C. P.; Cakir, Recep; Stoker, J. A.; Villeneuve, N. M.; Smith, D. T.; Bethel, J. P., 2012, Geologic map of the Lake Joy 7.5-minute quadrangle, King County, Washington: Washington Division of Geology and Earth Resources Map Series 2012-01, 2 sheets, scale 1:24,000, 79 p. text. [https://www.dnr.wa.gov/Publications/ger_ms2012-01_geol_map_lake_joy_24k.zip]

Dragovich, J. D.; Frattali, C. L.; Anderson, M. L.; Mahan, S. A.; MacDonald, J. H., Jr.; Stoker, B. A.; Smith, D. T.; Koger, C. J.; Cakir, Recep; DuFrane, S. A.; Sauer, K. B., 2014, Geologic map of the Lake Chaplain 7.5-minute quadrangle, Snohomish County, Washington: Washington Division of Geology and Earth Resources Map Series 2014-01, 1 sheet, scale 1:24,000, with 51 p. text. [https://www.dnr.wa.gov/Publications/ger_ms2014-01_geol_map_lake_chaplain_24k.zip]

Eddy, M. P.; Bowring, S. A.; Umhoefer, P. J.; Miller, R. B.; McLean, N. M.; Donaghy, E. E., 2016, High-resolution temporal and stratigraphic record of Siletzia's accretion and triple junction migration from nonmarine sedimentary basins in central and western Washington: Geological Society of America Bulletin, v. 128, no. 3–4, p. 425–441. [https://doi.org/10.1130/B31335.1]

Erikson, E. H., Jr., 1969, Petrology of the composite Snoqualmie batholith, central Cascade mountains, Washington: Geological Society of America Bulletin, v. 80, no. 11, p. 2213–2236, 1 plate. [https://doi.org/10.1130/0016-7606(1969)80[2213:POTCSB]2.0.CO;2]

Fairhall, A. W.; Schell, W. R.; Young, J. A., 1966, Radiocarbon dating at the University of Washington, III: Radiocarbon, v. 8, p. 498–506. [https://doi.org/10.1017/S003382220000031X]

Finn, C. A.; Phillips, W. M.; Williams, D. L., 1991, Gravity anomaly and terrain maps of Washington: U.S. Geological Survey Geophysical Investigations Map GP-988, 5 sheets, scale 1:500,000. [https://pubs.er.usgs.gov/publication/gp988]

Frizzell, V. A., Jr.; Tabor, R. W.; Zartman, R. E.; Blome, C. D., 1987, Late Mesozoic or early Tertiary mélanges in the western Cascades of Washington. *In* Schuster, J. E., editor, Selected papers on the geology of Washington: Washington Division of Geology and Earth Resources Bulletin 77, p. 129–148. [https://www.dnr.wa.gov/Publications/ger_b77_papers_on_wa_geology_pt2of3.pdf]

Fuller, R. E., 1925, The geology of the northeastern part of Cedar Lake quadrangle with special reference to the de-roofed Snoqualmie batholith: University of Washington Master of Science thesis, 96 p., 4 plates.

Hammond, P. E., 1963, Structure and stratigraphy of the Keechelus volcanic group and associated Tertiary rocks in the west-central Cascade Range, Washington: University of Washington Doctor of Philosophy thesis, 254 p., 2 plates.

Hammond, P. E.; Dragovich, J. D., 2008, Tuff of Stampede Pass and tuff of Green Canyon in the central Cascade Range, King and Kittitas Counties, Washington: Washington Division of Geology and Earth Resources Open File Report 2008-3, 8 p. text with 1 Excel file on DVD. [http://www.dnr.wa.gov/Publications/ger_ofr2008-3_stampedepass_greencanyon_tuff.zip]

Heiskanen, W. A.; Vening-Meinesz, F. A., 1958, The Earth and its gravity field: McGraw-Hill Book Company, Inc., 470 p.

Huntley, D. J.; Godfrey-Smith, D. I.; Thewalt, M. L. W., 1985, Optical dating of sediments: Nature, v. 313, p. 105–107. [https://doi.org/10.1038/313105a0]

Johnson, S. Y.; O'Connor, J. T., 1994, Stratigraphy, sedimentology, and provenance of the Raging River Formation (early? and middle Eocene), King County, Washington: U.S. Geological Survey Bulletin 2085-A, 33 p. [http://pubs.er.usgs.gov/publication/b2085A]

Kelsey, H. M.; Sherrod, B. L.; Nelson, A. R.; Brocher, T. M., 2008, Earthquakes generated from bedding plane-parallel reverse faults above an active wedge thrust, Seattle fault zone: Geological Society of America Bulletin, v. 120, n. 11–12, p. 1581–1597. [https://doi.org/10.1130/B26282.1]

King County, 2003, King 2003 project, 6-ft resolution, accessed June 15, 2021 [http://lidarportal.dnr.wa.gov/].

Koppers, A. A. P.; Staudigel, Hubert; Wijbrans, J. R., 2000, Dating crystalline groundmass separates of altered Cretaceous seamount basalts by the $^{40}Ar/^{39}Ar$ incremental heating technique: Chemical Geology, v. 166, no. 1–2, p. 139–158. [https://doi.org/10.1016/S0009-2541(99)00188-6]

Koppers, A. A. P., 2002, ArArCALC—Software for $^{40}Ar/^{39}Ar$ age calculations: Computers & Geosciences, v. 28, no. 5, p. 605–619. [https://doi.org/10.1016/S0098-3004(01)00095-4]

Koppers, A. A. P.; Staudigel, Hubert; Pringle, M. S.; Wijbrans, J. R., 2003, Short-lived and discontinuous intraplate volcanism in the South Pacific: Hot spots or extensional volcanism?: Geochemistry, Geophysics, Geosystems, v. 4, no. 10, 49 p. [https://doi.org/10.1029/2003GC000533]

Kuiper, K. F.; Deino, Alan; Hilgen, F. J.; Krijgsman, Wout; Renne, P. R.; Wijbrans, J. R., 2008, Synchronizing rock clocks of Earth history: Science, v. 320, no. 5875, p. 500–504. [https://doi.org/10.1126/science.1154339]

Lanphere, M A.; Baadsgaard, Halfdan, 2001, Precise K–Ar, $^{40}Ar/^{39}Ar$, Rb–Sr and U/Pb mineral ages from the 27.5 Ma Fish Canyon Tuff reference standard: Chemical Geology, v. 175, no. 3–4, p. 653–671. [https://doi.org/10.1016/S0009-2541(00)00291-6]

Lee, J.-Y.; Marti, Kurt; Severinghaus, J. P.; Kawamura, Kenji; Yoo, H.-S.; Lee, J. B.; Kim, J. S., 2006, A redetermination of the isotopic abundances of atmospheric Ar: Geochimica et Cosmochimica Acta, v. 70, no. 17, p. 4507–4512. [https://doi.org/10.1016/j.gca.2006.06.1563]

Liberty, L. M.; Pratt, T. L., 2008, Structure of the eastern Seattle fault zone, Washington State: New insights from seismic reflection data: Bulletin of the Seismological Society of America, v. 98, no. 4, p. 1681–1695. [https://doi.org/10.1785/0120070145]

Mackin, J. H., 1941, Glacial geology of the Snoqualmie–Cedar area, Washington: Journal of Geology, v. 49, no. 5, p. 449–481. [https://doi.org/10.1086/624984]

Mickelson, K. A.; Jacobacci, K. E.; Contreras, T. A.; Gallin, W. N.; Slaughter, S. L., 2019, Landslide inventory of western King County, Washington: Washington Geological Survey Report of Investigations 41, 7 p. text, with an accompanying Esri file geodatabase. [https://fortress.wa.gov/dnr/geologydata/publications/ger_ri41_western_king_county_landslide_inventory.zip]

Min, Kyoungwon; Mundil, Roland; Renne, P. R.; Ludwig, K. R., 2000, A test for systematic errors in $^{40}Ar/^{39}Ar$ geochronology through comparison with U-Pb analysis of a 1.1-Ga rhyolite: Geochimica et Cosmochimica Acta, v. 64, no. 1, p. 73–98. [https://doi.org/10.1016/S0016-7037(99)00204-5]

Morelli, Carlo; Gantar, C.; Honkasalo, Tauno; McConnel, R. K.; Tanner, J. G.; Szabo, Bela; Uotila, Urho; Whalen, C. T., 1974, The international gravity standardization net 1971 (IGSN71): International Association of Geodesy Special Publication No. 4, 194 p.

Mullineaux, D. R., 1965, Geologic map of the Black Diamond quadrangle, King County, Washington: U.S. Geological Survey Geologic Quadrangle Map GQ-407, 1 sheet, scale 1:24,000. [https://doi.org/10.3133/gq407]

Paces, J. B.; Miller, J. D., Jr., 1993, Precise U-Pb ages of Duluth Complex and related mafic intrusions, northeastern Minnesota: Geochronological insights to physical, petrogenetic, paleomagnetic, and tectonomagmatic processes associated with the 1.1 Ga Midcontinent Rift System: Journal of Geophysical Research, v. 98, no. B8, p. 13,997–14,013. [https://doi.org/10.1029/93JB01159]

Paton, Chad; Hellstrom, John; Paul, Bence; Woodhead, Jon; Hergt, Janet, 2011, Iolite: Freeware for the visualization and processing of mass spectrometric data: Journal of Analytical Atomic Spectrometry, v. 26, p. 2508–2518. [https://doi.org/10.1039/C1JA10172B]

Phillips, J. D.; Hansen, R. O.; Blakely, R. J., 2007, The use of curvature in potential-field interpretation: Exploration Geophysics, v. 38, p. 111–119. [https://doi.org/10.1071/EG07014]

Plouff, D., 2000, Field estimates of gravity terrain corrections and Y2K-compatible method to convert from gravity readings with multiple base stations to tide- and long-term drift-corrected observations: U.S. Geological Survey Open-File Report 00-140, 37 p. [https://pubs.usgs.gov/of/2000/0140/]

Porter, S. C., 1976, Pleistocene glaciation in the southern part of the North Cascade Range, Washington: Geological Society of America Bulletin, v. 87, no. 1, p. 61–75. [https://doi.org/10.1130/0016-7606(1976)87%3C61:PGITSP%3E2.0.CO;2]

PSLC, 2014, Cedar River B 2014 project, collected between October, 2013 and July, 2014 by Quantum Spatial Inc., 3-ft resolution, accessed June 15, 2021 [http://lidarportal.dnr.wa.gov/], metadata available on portal [ger_king_county_2016_lidar_report.pdf].

PSLC, 2016, King County 2016 project, collected between Feb. 24, 2016 and May 25, 2017 by Quantum Spatial Inc., 3-ft resolution, accessed June 15, 2021 [http://lidarportal.dnr.wa.gov/], metadata available on portal [ger_cedar_river_b_2014_lidar_report.pdf].

Rhodes, E. J., 2011, Optically stimulated luminescence dating of sediments over the past 200,000 years: Annual Review of Earth and Planetary Sciences, v. 39, p. 461–488. [https://www.annualreviews.org/doi/10.1146/annurev-earth-040610-133425]

Sláma, Jiří; Košler, Jan; Condon, D. J.; Crowley, J. L.; Gerdes, Alex; Hanchar, J. M.; Horstwood, M. S. A.; Morris, G. A.; Nasdala, Lutz; Norberg, Nicholas; Schaltegger, Urs; Schoene, Blair; Tubrett, M. N.; Whitehouse, M. J., 2008, Plešovice zircon—A new natural reference material for U-Pb and Hf isotopic microanalysis: Chemical Geology, v. 249, no. 1-2, p. 1–35. [https://doi.org/10.1016/j.chemgeo.2007.11.005]

Sherrod, B. L.; Blakely, R. J.; Weaver, C. S.; Kelsey, H. M.; Barnett, E.; Liberty, Lee; Meagher, K. L.; Pape, Kristin, 2008, Finding concealed active faults: Extending the southern Whidbey Island fault across the Puget Lowland, Washington: Journal of Geophysical Research, v. 113, no. B5, 25 p. [https://doi.org/10.1029/2007JB005060]

Smith, G. O.; Calkins, F. C., 1906, Snoqualmie folio, Washington: U.S. Geological Survey Folios of the Geologic Atlas 139, 14 p., with 13 maps, scale 1:125,000. [https://doi.org/10.3133/gf139]

Steiger, R. H.; Jäger, Emilie, 1977, Subcommission on geochronology: Convention on the use of decay constant in geo- and cosmochronology: Earth and Planetary Science Letters, v. 36, no. 3, p. 359–362. [https://doi.org/10.1016/0012-821X(77)90060-7]

Swick, C. H., 1942, Pendulum gravity measurements and isostatic reductions: U.S. Department of Commerce Coast and Geodetic Survey Special Publication 232, 82 p.

Tabor, R. W.; Frizzell, V. A., Jr.; Vance, J. A.; Naeser, C. W., 1984, Ages and stratigraphy of lower and middle Tertiary sedimentary and volcanic rocks of the central Cascades, Washington: Application to the tectonic history of the Straight Creek fault: Geological Society of America Bulletin, v. 95, no. 1, p. 26–44. [https://doi.org/10.1130/0016-7606(1984)95%3C26:AASOLA%3E2.0.CO;2]

Tabor, R. W.; Frizzell, V. A., Jr.; Booth, D. B.; Waitt, R. B.; Whetten, J. T.; Zartman, R. E., 1993, Geologic map of the Skykomish River 30- by 60-minute quadrangle, Washington: U.S. Geological Survey Miscellaneous Investigations Series Map I-1963, 1 sheet, scale 1:100,000, with 42 p. text. [http://pubs.usgs.gov/imap/i1963/]

Tabor, R. W.; Frizzell, V. A.; Booth, D. B.; Waitt, R. B., 2000, Geologic map of the Snoqualmie Pass 30 x 60 minute quadrangle, Washington: U.S. Geological Survey Geologic Investigation Series Map I-2538, 1 sheet, scale 1:100,000, and pamphlet. [http://geopubs.wr.usgs.gov/i-map/i2538/]

Telford, W. M.; Geldart, L. O.; Sheriff, R. E., 1990, Applied Geophysics: New York, Cambridge University Press, 770 p.

ten Brink, U. S.; Molzer, P. C.; Fisher, M. A.; Blakely, R. J.; Bucknam, R. C.; Parsons, T. E.; Crosson, R. S.; Creager, K. C., 2002, Subsurface geometry and evolution of the Seattle Fault zone and the Seattle basin, Washington: Seismological Society of America Bulletin, v. 92, no. 5, p. 1737–1753. [https://doi.org/10.1785/0120010229]

Thorson, R. M., 1981, Isostatic effects of the last glaciation in the Puget Lowland, Washington: U.S. Geological Survey Open-File Report 81-370, 100 p., 1 plate. [https://pubs.er.usgs.gov/publication/ofr81370]

Vermeesch, Pieter, 2018, IsoPlotR: A free and open toolbox for geochronology: Geoscience Frontiers, v. 9, no. 5, p. 1479–1493. [https://doi.org/10.1016/j.gsf.2018.04.001]

Vine, J. D., 1969, Geology and coal resources of the Cumberland, Hobart, and Maple Valley quadrangles, King County, Washington: U.S. Geological Survey Professional Paper 624, 67 p., 4 plates. [https://pubs.usgs.gov/pp/0624/report.pdf]

Wells, R. E.; Weaver, C. S.; Blakely, R. J., 1998, Fore-arc migration in Cascadia and its neotectonic significance: Geology, v. 26, no. 8, p. 759–762. [https://doi.org/10.1130/0091-7613(1998)026%3C0759:FAMICA%3E2.3.CO;2]

Wiedenbeck, Michael; Allé, P.; Corfu, Fernando; Griffin, W. L.; Meier, Martin; Oberli, Felix; Von Quadt, Albrecht; Roddick, J. C.; Spiegel, W., 1995, Three natural zircon standards for U-Th-Pb, Lu-Hf, trace element and REE analyses: Geostandards Newsletters, v. 19, p. 1–23. [https://doi.org/10.1111/j.1751-908X.1995.tb00147.x]

Williams, I. S., 1998, U-Th-Pb geochronology by ion microprobe. *In* McKibben, M. A.; Shanks III, W. C.; Ridley, W. I., editors, Applications of microanalytical techniques to understanding mineralizing processes: Reviews in Economic Geology, v. 7, p. 1–35. [https://doi.org/10.5382/Rev.07.01]

Appendix A. Geochronology

^{40}AR/^{39}AR ARGON DATING

Overview

Argon dating uses the radioactive decay of ^{40}K to ^{40}Ar to determine the age of potassium-bearing minerals and materials. In this map area we use ^{40}Ar/^{39}Ar argon dating to try and establish the crystallization age of the intrusive rock of the Snoqualmie batholith and a number of flows and tuffs throughout the Eocene to Oligocene volcanic succession. Because of the presence of younger (Oligocene to Miocene) intrusive rocks in the region, we were concerned about heat from the intrusions affecting the argon ages. This problem has been noted by past workers (Dragovich and others, 2009a; Tabor and others, 2000). Thus, we employ both argon and U-Pb dating (which is not affected by heat in the same way) and also date one location (age site GD9–10) with both methods.

Sample Collection and Preparation

Samples for argon dating need to be recovered from in-place volcanic rock and should have as little weathering and alteration as possible. We prioritized sites where rock was relatively unweathered and had few fractures, though such sites were very difficult to find in this area. Large blocks of the outcrop were removed and broken into smaller pieces in order to remove any weathering rinds on the rock. We placed about 1–3 kg of rock into a cloth or sturdy plastic sample bag. At the conclusion of field work, sites from which samples were collected were ranked based on many factors, including the desire for spatial coverage, stratigraphic location, rock type, and budgetary constraints. Of those samples to be analyzed, we selected the freshest pieces and sent 1–2 kg of material to the lab for irradiation and analysis.

Analytical methods

The following section of text is reproduced from an analytical report provided by the Oregon State University Argon Geochronology Laboratory, with minimal modification:

Samples were crushed, sieved, washed, and dried using standard mineral separation techniques. Groundmass splits were obtained for the sample, rinsed with cold water, and then dried in a drying oven at 55 °C. Once the samples were dried, they were sieved to 250–150 µm. Special care was taken to remove any alteration material by using an intensive acid leaching procedure using a combination of HCl and HNO_3 at different acid strength (Koppers and others, 2000). A final separate of groundmass was obtained using a binocular microscope. Any visible alteration or adhering crystal phases were carefully removed prior to packaging and irradiation of the sample.

^{40}Ar/^{39}Ar ages were obtained by incremental heating methods using the ThermoFisher Scientific ARGUS-VI mass spectrometer and data collection using internal lab software ArArExperiments version 4.4.0. The samples were irradiated for 6 hours. Samples were irradiated with the Fish Canyon Tuff sanidine (FCT-2-NM sanidine) with an age of 28.201 ±0.023 Ma, 1σ flux monitor (Kuiper and others, 2008). Individual J-values for each sample were calculated by polynomial extrapolation of the measured flux gradient against irradiation height and typically give 0.06–0.12 percent uncertainties (1σ). The ^{40}Ar/^{39}Ar incremental heating age determinations were performed on a multi-collector ARGUS-VI mass spectrometer at Oregon State University that has five Faraday collectors fitted, two 1,012 ohm resistors for masses ^{41}Ar and ^{40}Ar and three 1,013 ohm resistors for argon masses ^{39}Ar, ^{38}Ar, and ^{37}Ar and one ion-counting CuBe electron multiplier (located in a position next to the lowest mass Faraday collector). This allows us to measure simultaneously all argon isotopes, with mass 36 on the multiplier and masses 37 through 40 on the four adjacent Faradays. This configuration provides the advantages of running in a full multi-collector mode while measuring the lowest peak (on mass 36) on the highly sensitive electron multiplier (which has an extremely low dark-noise and a very high peak/noise ratio). Irradiated samples were loaded into Cu-planchettes in an ultra-high vacuum sample chamber and incrementally heated by scanning a Synrad Firestar 20-watt defocused CO_2 laser beam in pre-set patterns across the sample, in order to release the argon evenly. Each heating step is 62 seconds. After heating, reactive gasses were cleaned up using four SAES Zr-Al AP10 getters for 3 minutes; two operated at 450°C and two operated at room temperature (21°C). All ages were calculated using the corrected Steiger and Jäger (1977) decay constant of 5.530 ±0.097 x 10^{-10} yr^{-1} (2σ) as reported by Min and others (2000). For all other constants used in the age calculations we refer to table 2 in Koppers and others (2003). Incremental heating plateau ages and isochron ages were calculated as weighted means with 1/σ2 as weighting factor and as YORK2 least-square fits with correlated errors using the ArArCALC v2.6.2 software from Koppers (2002) available from the website at http://earthref.org/ArArCALC/.

Argon isotopic results are corrected for system blanks, radioactive decay, mass discrimination, reactor-induced interference reactions, and atmospheric argon contamination. Decay constants reported by Min and others (2000) are utilized for age calculation. Isotope interference corrections as determined using the ARGUS VI are: (^{36}Ar/^{37}Ar)Ca=0.0002703 ±0.000005; (^{39}Ar/^{37}Ar)Ca=0.0006425 ±0.0000059; (^{40}Ar/^{39}Ar)K= 0.000607 ±0.000059; (^{38}Ar/^{39}Ar)K=0.012077 ±0.000011. Ages were calculated assuming an atmospheric ^{40}Ar/^{36}Ar ratio of 298.56 ±0.113 (Lee and others, 2006). Data reduction and age calculation were processed using ^{40}Ar/^{39}Ar Calc 2.7.0 (Koppers, 2002). Plateau ages are defined as including >50% of the total ^{39}Ar released with at least three

consecutive steps, where the $^{40}Ar/^{39}Ar$ ratio for each step is in agreement with the mean at the 95% confidence level. In many cases only a mini-plateau age is given, where a mini-plateau is <50% of the ^{39}Ar released.

Results

We collected and analyzed seven samples: three are from tuffs, three are from basalt to andesite flows, and one is an intrusive gabbro. Summary data are in Table 1 and Table A1; analytical data are in the Data Supplement.

Table A1. Argon geochronology sample information and results. Uncertainties are provided at 2-sigma unless otherwise noted. Ages are reported with internal uncertainty, followed by full external uncertainty in parentheses.

Sample ID (map ID)		Plateau age (Ma)	% total ^{39}Ar included in age	Number of heating steps included in age	MSWD
AS20SEP21-7 (GD5)		a. 21.01 ±0.10 (±1.09) b. 24.80 ±0.08 (±1.29) c. 25.24 ±1.01 (±1.65)	a. 40 b. 92 c. 86	a. 7 b. 27 c. 18	a. 0.79 b. 1.96 c. 0.81
Lab ID	a. OSU_22F08215 b. OSU_22F08450 c. OSU_22F06458	From back wall of abandoned quarry near DNR Fire Training Academy. Light gray to white with abundant dark brown mafic minerals; medium-grained equigranular intrusive rock			
TRS	sec. 28, T23N R9E				
Lat/long. (degrees)	47.453066 -121.654405				
Elev. (ft)	1,662				
Material	a. plagioclase b. biotite c. groundmass				
Geologic unit	ᗰᗣii				
Geochemical classification	Gabbro				
AS23SEP21-6 (GD9)		22.86 ±0.05 (±1.19)	55	16	3.56
Lab ID	OSU_22F05882	From cliff exposure along Mount Washington trail. Light gray with some light green; mostly groundmass with abundant scattered plagioclase crystals and local subtle mineral clumps or possible volcanic clasts; locally contains small irregular quartz grains.			
TRS	sec. 29, T23N R9E				
Lat/long. (degrees)	47.441047 -121.678523				
Elev. (ft)	1,540				
Material	groundmass				
Geologic unit	ᗣEv (tuff)				
Geochemical classification	Dacitic rhyolite				
AS23JUL21-2 (GD14)		28.72 ±0.08 (±1.49)	53	13	1.01
Lab ID	OSU_22F05816	From logging roadcut west of summit of Mount Washington. Sample from a grayish-tan 2-m-thick fine-grained layer with local oblong to round cavities that could be vesicles. Layer is within an otherwise homogenous outcrop of blue-green angular cobble to boulder tuff breccia. Field relationships do not clearly indicate whether the sampled layer is a sill, a flow, or a tuff.			
TRS	sec. 31, T23N R9E				
Lat/long. (degrees)	47.428177 -121.704901				
Elev. (ft)	4,110				
Material	groundmass				
Geologic unit	ᗣEv (tuff)				
Geochemical classification	Andesite				

Table A1 continued. Ages are reported with internal uncertainty, followed by full external uncertainty in parentheses.

Sample ID (map ID)		Plateau age (Ma)*	% total 39Ar included in age	Heating steps included in age	MSWD
AS19AUG21-1 (GD17)		31.91 ±0.07 ±1.65	64	15	0.97
Lab ID	OSU_22F06570	From logging roadcut near Chester Morse Lake. Dark gray to slightly green; nearly aphanitic; identified in the field as basalt; locally contains trace amounts of pyrite.			
TRS	sec. 7, T22N R9E				
Lat/long. (degrees)	47.407068 -121.709554				
Elev. (ft)	1,612				
Material	groundmass				
Geologic unit	ΦEv (flow)				
Geochemical classification	Andesite				
AS26JUL21-2 (GD18)		32.90 ±0.17 ±1.71	67	18	1.42
Lab ID	OSU_22F06094	From logging roadcut east of Damburrat Creek. Dark gray to dark blue or green; aphanitic groundmass with abundant (up to 30%) plagioclase up to 1.5 mm long; identified in the field as basalt; chalcedony locally fills vugs and small fractures.			
TRS	sec. 11, T22N R8E				
Lat/long. (degrees)	47.402282 -121.745756				
Elev. (ft)	2,600				
Material	groundmass				
Geologic unit	ΦEv (flow)				
Geochemical classification	Basaltic andeste				
AS24AUG21-10 (GD19)		18.44 ±0.05 ±0.96	16	4	2.19
Lab ID	OSU_22F05927	From expansive logging roadcut and cliff east of McClellan Creek. Sampled flow is on the north side of the outcrop belt and is about 3 m thick, dark gray, microcrystalline to aphanitic, locally vesicular, and locally has crude columnar jointing. This layer is within a package of other similar-looking, but somewhat more altered flows.			
TRS	sec. 15, T22N R9E				
Lat/long. (degrees)	47.387784 -121.647483				
Elev. (ft)	3,207				
Material	groundmass				
Geologic unit	ΦEv (flow)				
Geochemical classification	Basaltic trachyandesite				
AS25AUG21-4 (GD20)		25.60 ±0.08 ±1.33	9	8	0.48
Lab ID	OSU_22F05989	From logging roadcut west of Rack Creek. White, light gray, or light green; abundant plagioclase phenocrysts up to several mm long; locally abundant but typically sparse pebble- to rare cobble-size clasts of volcanic rock; identified in the field as a vitric-crystal tuff.			
TRS	sec. 23, T22N R8E				
Lat/long. (degrees)	47.383151 -121.740454				
Elev. (ft)	2,640				
Material	groundmass				
Geologic unit	ΦEv (tuff)				
Geochemical classification	Dacite				

U-PB ZIRCON DATING

Overview

Zircons are common accessory minerals in igneous rocks. Because they are hard and chemically inert, zircons often last through many rock cycles and are common constituents of most sedimentary, metamorphic, and igneous rocks. Decay of trace uranium to lead within zircon can be used to establish an individual age for each grain. Analyzing many grains (>50) within a sample can do two things: (1) establish a maximum depositional age based on the idea that the deposit must be younger than the youngest grain it contains, and (2) the variety of ages in a single sample can provide insight into the provenance of the sample.

In this map we use zircon dating for several purposes. The first is to establish the crystallization age of rocks we expect to have been re-heated by the abundant Oligocene to Miocene intrusive rocks. Such reheating can affect argon ages, so zircon dating (which is not affected in the same way) is a better approach. We also use zircon dating to understand the age and provenance of sandstone units. And lastly we use zircon dating to constrain the eruptive age of pyroclastic lapilli tuff deposits from the Eocene to Oligocene Cascade volcanic arc.

Sample collection and preparation

Because weathering and alteration do not affect the age of zircon, our samples are selected primarily upon our desire to understand the ages of particular rock units. In general, we attempt to retrieve about 2–4 kg of fresh rock for each sample, making sure to minimize any contact with soil or other surface deposits which could introduce anomalous zircons. The packaged samples are sent to ZirChron, LLC for mineral separation using the following procedure: Samples are pressure washed with water and then disaggregated using an Electro Pulse Disaggregator (EPD, Marx generator) at 1 Hz with discharges of ~250 kV for 15 minutes. Any clasts >500 µm are crushed in a crusher or pulverizer. Using stainless steel sieves, the fraction between 350 µm and 25 µm is retained and then processed using the Wilfley water table, Frantz paramagnetic separator, and a two-step (3.00 g/cm^3 and 3.32 g/cm^3) heavy liquid methylene iodide separation. Zircon grains from each sample are hand selected and mounted in epoxy, polished to expose the grain centers, and regions suitable for analysis are identified from optical imaging.

Analytical Methods

The following text is reproduced from a technical write-up by the Washington State University Radiogenic Isotope and Geochronology Laboratory with minimal modification:

Zircon U-Pb ages are measured at the Radiogenic Isotope and Geochronology Lab (RIGL) at Washington State University using an Analyte G2 193 excimer laser ablation system coupled with a Thermo-Finnigan Element 2 single-collector inductively coupled plasma mass spectrometer. The laser parameters are 25-µm-diameter spot size, 10 Hz repetition rate, and fluence of ~5.0 J/cm^2. For the U-Pb measurement, we mostly followed the method of Chang and others (2006), except for the use of a 193-nm laser system. A 10-second blank measurement of the He and Ar carrier gasses (laser off) before each analysis is followed by 250 scans across masses ^{202}Hg, ^{204}Pb+Hg, ^{206}Pb, ^{207}Pb, ^{208}Pb, ^{232}Th, ^{235}U and ^{238}U during ~30-second laser ablation period. Analyses of zircon unknowns, standards, and quality control zircon grains are interspersed with analyses of external calibration standards, typically with 10–12 unknowns bracketed by multiple analyses of two different zircon standards (Plešovice and FC-1). The Plešovice standard (337 Ma; Sláma and others, 2008) is used to calibrate the ^{206}Pb/^{238}U and ^{207}Pb/^{235}U ages, and the FC-1 standard (1,099 Ma; Paces and Miller, 1993) is used for calibration of ^{207}Pb/^{206}Pb ages owing to its high-count rate for ^{207}Pb (~2–4 times higher than that of Plešovice). Zircon 91500 (1,065 Ma; Wiedenbeck and others, 1995), Fish Canyon Tuff (~27.5 Ma; Lanphere and others, 2001) and Temora2 (417 Ma; Black and others, 2004) are used as quality control standards. Data are processed offline using the Iolite software (Paton and others, 2011). Common Pb correction is performed using the ^{207}Pb method (Williams, 1998).

Results

We collected seven samples for mineral separation but one did not yield zircon and this is not shown on the map or reported in our analytical data; the sample was located in a lapilli tuff from unit ΦEv at 47.417°N, -121.651°W. Of the remaining six samples, two are from sandstone, two are from intrusive gabbro, and two are from tuffs. Isochron ages, weighted-mean ages, concordia ages, and discordance filters (-5% to +15%) were made using IsoPlotR (Vermeesch, 2018). Summary data are in Table 1 and Table A2; individual zircon ages and analytical data are in the Data Supplement.

Table A2. U-Pb geochronology sample information and results. Uncertainties are provided at 2-sigma unless otherwise noted.

Sample ID (map ID)		Age ±2σ (Ma)	Age type
AS23SEP21-5 (GD2)		155.79 ±0.35	Concordia age (n=51)
TRS	sec. 11, T23N R8E	From natural outcrop along Old 444th Ave. Gray to slightly greenish; medium-grained intrusive rock with abundant thin chloritic shear zones and bands; locally has incipient to moderately developed foliation; identified in the field as diorite or quartz diorite.	---
Lat/long. (degrees)	47.485588 -121.74581		
Elev. (ft)	637		
Number of grains analyzed	51		
Geologic unit	Jiw		
AS05SEP21-3 (GD8)		86.54 ±0.96	Weighted mean (n=2)
TRS	sec. 30, T23N R9E	From bedrock in South Fork Snoqualmie River just off the Twin Falls trail. Dark gray to bluish gray; 2-m-thick structureless fine sandstone interbedded with 2–20-cm-thick black shale; the shale is locally contorted; the sandstone does not appear deformed but has abundant 1–10-mm-wide calcite veins with a range of orientations.	Uses two youngest grains; seven grains are <90 Ma.
Lat/long. (degrees)	47.445812 -121.699104		
Elev. (ft)	706		
Number of grains analyzed	108		
Geologic unit	KJmsw		
AS23SEP21-6 (GD10)		34.66 ±0.10	Weighted mean (n=104)
TRS	sec. 29, T23N R9E	From cliff exposure along Mount Washington trail. Light gray with some light green; mostly groundmass with abundant scattered plagioclase crystals and local subtle mineral clumps or possible volcanic clasts; locally contains small irregular quartz grains.	Uses all Eocene grains without a discordance filter. A concordia age for these same grains is 34.49 ±0.09 Ma.
Lat/long. (degrees)	47.441047 -121.678523		
Elev. (ft)	1,540		
Number of grains analyzed	108		
Geologic unit	ΦEv		
AS23SEP21-10 (GD13)		152.97 ±0.34	Concordia age (n=44)
TRS	sec. 35, T23N R9E	From west end of roadcut along Interstate 90. Light gray fine to medium-grained intrusive rock identified in the field as diorite; lacks evidence for greenschist-facies metamorphism.	Five grains rejected due to discordance.
Lat/long. (degrees)	47.429397 -121.62714		
Elev. (ft)	1,340		
Number of grains analyzed	49		
Geologic unit	Jiw		
AS22SEP21-1 (GD15)		<47.20 ±0.39	Weighted mean (n=3)
TRS	sec. 1, T22N R8E	From 2-m-tall roadcut along abandoned logging road 105. Sample is from a tan to brown and orange 20-cm-thick medium-grained well-sorted lithic sandstone low-angle and low-amplitude cross beds are present in the lower 4–5 cm of the sampled layer Below this is a 1-m-thick gritty to sparse pebbly sandstone. Capping the outcrop is a sandy pebble conglomerate; clasts are sub rounded to angular; rounded clasts are typically dark chert; more-angular clasts are typically off-white to green tuffaceous rock.	Uses three youngest grains; weighted mean of youngest seven grains is 47.72 ±0.25 Ma.
Lat/long. (degrees)	47.425455 -121.728679		
Elev. (ft)	1,767		
Number of grains analyzed	112		
Geologic unit	Ecg		
AS21SEP21-4 (GD16)		34.47 ±0.09	Weighted mean (n=97)
TRS	sec. 8, T23N R9E	From roadcut near summit of Greenway Mountain. Sample is from light green to light or dark blue lithic lapilli tuff; overlain by crudely columnar brown to gray pumice-rich lapilli tuff; both rock types are intruded by 0.75-m-thick dike of brownish green fine-grained rock with small quartz eyes and fine-grained mafic minerals.	Uses all Eocene grains without a discordance filter. A concordia age for these same grains is 34.63 ±0.09 Ma.
Lat/long. (degrees)	47.407876 -121.680376		
Elev. (ft)	4,401		
Number of grains analyzed	99		
Geologic unit	ΦEv		

LUMINESCENCE DATING

Overview

Natural radiation within sand deposits causes electrons to be trapped within the crystal lattice of quartz grains or feldspar grains (Rhodes, 2011). When shielded from heat and light, electrons accumulate through time at known rates. Measuring the number of electrons that have accumulated in a sand sample is the basis for determining the amount of time since the deposit was buried (Huntley and others, 1985). Dating quartz grains is accomplished by stimulating the grains with a laser light source and is referred to as Optically Stimulated Luminescence dating (OSL); dating feldspar grains uses an infrared light source and is referred to as Infrared-Stimulated Luminescence dating (IRSL).

We can use both types of luminescence dating to establish the burial age of Quaternary deposits that we find stratigraphically beneath glacial deposits of Vashon age (the most-recent glaciation). Dating these deposits helps to determine if they are from a previous glacial or interglacial period. Also, because pre-Vashon-age deposits are locally faulted and tilted, determining their age helps in constraining the timing of their deformation.

Sample collection and preparation

We collect samples from outcrops that meet the following criteria: (1) fine- to medium-grained sand with a moderate quartz and (or) feldspar content; (2) bed thickness greater than 10 cm (and hopefully greater than 30 cm); (3) avoid areas of bioturbation or obvious mechanical mixing; (4) sample site is at least 1 m (and preferably >2 m) below the top of the deposit. Criteria 1 ensures that the correct type of material is sampled; criteria 2–4 ensure that the calculated age is as close to the burial age as possible.
Once a suitable site is located, we scrape several cm of sediment off the face of the deposit to reveal fresh sediment. We prepare the sampling tube (nominal 4-cm-diameter metal tube about 20 cm long with one sharpened end) by placing a thin foam disc into it (this helps to keep the sediment in place during transit). We insert the tube into the deposit and use a sledge hammer and metal insert—placed between the hammer and the tube, to keep from damaging the tube—to fully push the tube into the outcrop. Once the tube is fully inserted, we cover and tape the exposed end. We collect about 1 kg of sand from a 10 cm by 10 cm area around the sample tube and place this material into a large sample bag. We also collect about 50–100 mL of the sand and place this into a small, sealed container. The large sample of sand is used to determine dose rate, and the small sample is for determining moisture content. The sample tube is then carefully removed from the outcrop and the other end is quickly covered and taped. A full suite of material (sealed tube, large sample of sand, and small sample of sand) is sent to the lab for analysis.

Analytical methods

Our samples are analyzed by the luminescence lab at the Illinois State Geological Survey and a detailed report on their methods is in the Data Supplement.

Results

We collected and analyzed four samples using both OSL and IRSL techniques. A summary of ages is in Table 1 and Table A3; detailed results are in the Data Supplement.

Table A3. Luminescence geochronology sample information and results. Uncertainties are provided at 2-sigma unless otherwise noted.

Sample ID (map ID)		Number of Aliquots (accepted of total)	Grain size(µm)	Equivalent dose (Gy)	Total dose rate (Gy/ka)	Age ±2σ (ka)
AS05SEP21-5 (GD3)		12 of 12	150–250	67 ±4	3.12 ±0.10	21.5 ±1.6
Lab ID	803	From roadcut along Lake Dorothy Road. There was likely a significant amount of sediment originally deposited above the sample perhaps tens of meters. Younger fluvial terraces incised into the deposit and the base of one of these incised terraces is 70 cm above the sample site. The sampled unit is compact tan fine sand with dispersed sparse pebbles. The sample is 55 cm from a large angular boulder.				
TRS	sec. 17, T23N R9E					
Lat/long. (degrees)	47.472853 -121.688818					
Elev. (ft)	821					
Material	sand					
Geologic unit	Qguc					
AS5SEP21-4 (GD4)		10 of 21	150–250	89 ±7	2.23 ±0.08	40.0 ±3.4
Lab ID	802	From tall cliff along the South Fork Snoqualmie River. Sample is from a 15 cm normally graded medium to fine sandstone interbedded with thinly bedded fine sand and clayey silt (below) and a medium bed of clayey silt (above). About 1 m above high-river level near base of 11-m-tall cliff. Cliff is composed of rythmically bedded or varved sediment dipping about 55 degrees northeast; sample is from near the base of the observed stratigraphy.				
TRS	sec. 24, T23N R8E					
Lat/long. (degrees)	47.461624 -121.723891					
Elev. (ft)	568					
Material	sand					
Geologic unit	Qguc					
AS5SEP21-1 (GD6)		11 of 93	150–250	96 ±10	2.26 ±0.08	42.3 ±4.7
Lab ID	800	From a deeply vegetated roadcut along 466th Place SE. Sample is from an 18-cm-thick fine- to medium-grained sand lens faulted between beds of tan clayey silt to very fine sand. Sample is about 1 m uphill from the main exposure, which consists of faulted dark bluish clay and tan medium-grained sand lenses. Sample is 3–4 m from top of cliff exposure and appears to lie beneath kettled ice-contact terrain (although this contact is inferred).				
TRS	sec. 25, T23N R8E					
Lat/long. (degrees)	47.448963 -121.720699					
Elev. (ft)	706					
Material	sand					
Geologic unit	Qguc					
AS5SEP21-2 (GD7)		12 of 23	150–250	109 ±11	2.23 ±0.08	49.1 ±5.4
Lab ID	801	From along the Twin Falls trail, about 700 ft north of the bridge. Sample is from a 30-cm-thick interval of fine sand. Above lies 15 cm of fine to medium sand with a pebbly base, above which is tan thinly bedded to laminated clayey siltstone. Water was actively dripping from top of clayey layer when sampled in late September.				
TRS	sec. 30, T23N R9E					
Lat/long. (degrees)	47.447031 -121.698107					
Elev. (ft)	885					
Material	sand					
Geologic unit	Qguc					

^{14}C DATING

Overview

Carbon-14 (^{14}C) dating uses the radioactive decay of ^{14}C to ^{13}C, the half-life of which is about 5,500 yrs. This makes the technique useful for dating carbon-containing objects less than about 35,000 years old. We use ^{14}C dating on charcoal and organic material within sedimentary units to help constrain their age of deposition.

Sample collection and preparation

Where charcoal or other organic material were found within sedimentary units, we carefully scraped off several centimeters of the exposure to reveal fresh portions of the deposit. The carbonaceous material was then carefully picked out by hand or with tweezers and placed into a sturdy plastic sample bag. Ideally, the sample was then enclosed in a secondary hard-sided container to ensure the material was not further disaggregated. We attempted to gather at least 0.5 g of material. The sample was then packaged and mailed to the lab for analysis.

Analytical methods

The following text is reproduced with little modification from the Beta Analytic website and describes the general procedure they follow. A more-detailed white paper on their method can be found at https://www.radiocarbon.com/PDF/AMS-Methodology.pdf. Before radiocarbon dating, the sample is first gently crushed then dispersed in deionized water. It is then washed with hot HCl acid to eliminate carbonates followed by an alkali wash (NaOH) to remove secondary organic acids. The alkali wash is followed by a final acid rinse to neutralize the solution before drying. Chemical concentrations, temperatures, exposure times, and number of repetitions depend on the sample submitted. Each chemical solution is neutralized prior to application of the next. During these serial rinses, mechanical contaminants such as associated sediments and rootlets are eliminated.

Treated samples are then analyzed by Accelerator Mass Spectrometry (AMS). The AMS measurement is done on graphite produced by hydrogen reduction of the CO_2 sample over a cobalt catalyst. The CO_2 is obtained from the combustion of the sample at 800°C+ under a 100 percent oxygen atmosphere. The CO_2 is first dried with methanol/dry ice then collected in liquid nitrogen for the subsequent graphitization reaction. The identical reaction is performed on reference standards, internal QA samples, and backgrounds to ensure systematic chemistry.

The analytical result is obtained by measuring sample ^{14}C/^{13}C relative to the ^{14}C/^{13}C in Oxalic Acid II (NIST-4990C) in one of Beta Analytic's multiple in-house particle accelerators using SNICS ion source. Quality assurance (QA) samples are measured along with the unknowns and reported separately in a 'QA report'. The radiocarbon dating lab requires results for the QA samples to fall within expectations of the known values prior to accepting and reporting the results for any given sample.

The AMS result is corrected for total fractionation using machine graphite δ^{13}C. The δ^{13}C reported for the sample is obtained by different ways depending upon the sample material. Solid organics are sub-sampled and converted to CO_2 with an elemental analyzer (EA). Water and carbonates are acidified in a gas bench to produce CO_2. Both the EA and the gas bench are connected directly to an isotope-ratio mass spectrometer (IRMS). The IRMS performs the separation and measurement of the CO_2 masses (44, 45, and 46) and calculation of the sample δ^{13}C.

Results

We collected and analyzed two samples; a summary of ages is in Table 1 and Table A4; detailed results are in the Data Supplement.

Table A4. C-14 geochronology sample information and results. Uncertainties are provided at 2-sigma unless otherwise noted.

Sample ID (map ID)		Age (^{14}C yr BP)	Calibrated age (cal yr BP)	Calibrated age probability	δ^{13}C (‰)
AS6SEP21-4 (GD1)		7,160 ±30	8,022–7,934	95.40%	-22.6
Lab ID	Beta-615854	From 2-m-tall outcrop along Granite Lakes trail. Tan to gray; poorly sorted; clay to grit with sparse small pebbles and abundant charcoal; predominantly silt to sand; competent; interpreted in the field as a fine-grained debris flow.			
TRS	sec. 11, T23N R9E				
Lat/long. (degrees)	47.487424 -121.635286				
Elev. (ft)	1,172				
Material	charcoal				
Geologic unit	Qgoa$_2$				

AS23SEP21-1 (GD11)		9,140 ±30	10,406–10,230	95.40%	-22.6
Lab ID	Beta-615855	From a roadcut along the abandoned Garcia Road just north of Interstate 90. Gray thinly bedded to thickly laminated medium- to fine-grained silty sand interbedded with thin tan sandy silt beds, a poorly sorted clay to pebble layer, and gritty coarse sand and sparse pebbles; all generally very hard. Outcrop is capped by at least 1–2 m of hard gray to tan diamicton. Charcoal is locally found throughout the outcrop; sample collected from sediment just below the diamicton.			
TRS	sec. 34, T23N R9E				
Lat/long. (degrees)	47.439727 -121.650555				
Elev. (ft)	1,314				
Material	charcoal				
Geologic unit	Qgl				

Appendix B. Geochemistry

OVERVIEW

We use major- and trace-element analyses to classify igneous rocks in the map area and aid in their identification and correlation. Although we only analyzed eight samples in this report, they span a range of rock types and are dispersed throughout the Eocene to Oligocene volcanic succession.

SAMPLE COLLECTION AND PREPARATION

We select samples for geochemical analysis from volcanic and intrusive rocks where we also determine ages. Large samples are collected in the field and a small sledge hammer is used to break off the freshest pieces. We submit a minimum of ~120 g of fresh material for lab analysis.

ANALYTICAL METHODS

We reproduce the following abbreviated methods directly from documents provided by the ALS Geochemistry Laboratory in Vancouver, British Columbia; only general descriptions of methods are provided by ALS on their website:

Major-element percentages are determined on a fused bead after acid digestion using Inductively Coupled Plasma-Atomic Emission Spectroscopy (ICP-AES)(ALS analysis code ME_ICP06). A prepared sample (0.1 g) is added to lithium metaborate/lithium tetraborate flux, mixed well, and fused in a furnace at 1,025°C. The resulting melt is then cooled and dissolved in an acid mixture containing nitric, hydrochloric, and hydrofluoric acids. This solution is then analyzed by ICP-AES. Results are corrected for spectral inter-element interferences and reported.

Loss on Ignition (LOI)(ALS analysis code OA_GRA05) is determined using a 1 g sample, placed in an oven at 1,000°C for one hour, cooled, and then weighed again. The percent loss on ignition is calculated from the difference in weight before and after ignition.

Trace element concentrations are determined using ICP-MS (ALS analysis code ME_MS81). Samples are prepared following the same lithium borate fusion and digestion procedure as applied in ICP-AES analyses, but are subjected to an additional lithium borate fusion and an acid digestion procedure prior to analysis on the ICP-MS.

RESULTS

We obtained results for eight samples. A summary geochemical classification is in Table 1; location data are in Table B1; analytical data are in the Data Supplement.

Table B1. Geochemistry sample information and summary classification based on the Total-Alkali-Silica diagram of LeMaitre and others (2002).

Sample ID (map ID)		Geochemical classification	Co-located analyses
20SEP21-7 (G1)		Gabbro	GD5; TS8
TRS	sec. 11, T23N R9E	From back wall of abandoned quarry near DNR Fire Training Academy. Light gray to white with abundant dark brown mafic minerals; medium-grained equigranular intrusive rock identified in the field as tonalite	
Lat/long. (degrees)	47.45307 -121.6544		
Elev. (ft)	1,662		
Geologic unit	MΦii		
23SEP21-6 (G2)		Dacitic rhyolite	GD9; GD10: TS10
TRS	sec. 11, T23N R8E	From cliff exposure along Mount Washington trail. Light gray with some light green; mostly groundmass with abundant scattered plagioclase crystals and local subtle mineral clumps or possible volcanic clasts; locally contains small irregular quartz grains.	
Lat/long. (degrees)	47.44105 -121.67852		
Elev. (ft)	1,540		
Geologic unit	ΦEv (tuff)		
23SEP21-10 (G3)		Gabbro	GD13
TRS	sec. 35, T23N R9E	From west end of roadcut along Interstate 90. Light gray fine- to medium-grained intrusive rock identified in the field as diorite; lacks evidence for greenschist-facies metamorphism.	
Lat/long. (degrees)	47.4294 -121.62714		
Elev. (ft)	1,340		
Geologic unit	Jiw		
23JUL21-2 (G4)		Andesite	GD14; TS19
TRS	sec. 31, T23N R9E	From logging roadcut west of summit of Mount Washington. Sample from a grayish-tan 2-m-thick fine-grained layer with local oblong to round cavities that could be vesicles. Layer is within an otherwise homogenous outcrop of blue-green angular cobble to boulder tuff breccia. Field relationships do not clearly indicate whether the sampled layer is a sill, a flow, or a tuff.	
Lat/long. (degrees)	47.42818 -121.7049		
Elev. (ft)	4,110		
Geologic unit	ΦEv (tuff)		
19AUG21-1 (G5)		Andesite	GD18; TS24
TRS	sec. 7, T22N R9E	From logging roadcut near Chester Morse Lake. Dark gray to slightly green; nearly aphanitic; identified in the field as basalt; locally contains trace amounts of pyrite.	
Lat/long. (degrees)	47.40707 -121.70955		
Elev. (ft)	1,612		
Geologic unit	ΦEv (flow)		
26JUL21-2 (G6)		Basaltic andesite	GD19; TS26
TRS	sec. 11, T22N R8E	From logging roadcut east of Damburrat Creek. Dark gray to dark blue or green; aphanitic groundmass with abundant (up to 30%) plagioclase up to 1.5 mm long; identified in the field as basalt; chalcedony locally fills vugs and small fractures.	
Lat/long. (degrees)	47.40228 -121.74576		
Elev. (ft)	2,600		
Geologic unit	ΦEv (flow)		
24AUG21-10 (G7)		Basaltic trachyandesite	GD20; TS29
TRS	sec. 15, T22N R9E	From expansive logging roadcut and cliff east of McClellan Creek. Sampled flow is on the north side of the outcrop belt and is about 3 m thick, dark gray, microcrystalline to aphanitic, locally vesicular, and locally has crude columnar jointing. This layer is within a package of other similar-looking, but somewhat more altered flows.	
Lat/long. (degrees)	47.38778 -121.64748		
Elev. (ft)	3,207		
Geologic unit	ΦEv (flow)		
25AUG21-4 (G8)		Dacite	GD21; TS32
TRS	sec. 23, T22N R8E	From logging roadcut west of Rack Creek. White, light gray, or light green; abundant plagioclase phenocrysts to several mm; locally abundant but typically sparse pebble- to rare cobble-size clasts of volcanic rock; identified in the field as a vitric-crystal tuff.	
Lat/long. (degrees)	47.38315 -121.74045		
Elev. (ft)	2,640		
Geologic unit	ΦEv (tuff)		

Appendix C. Geophysics

GRAVITY

Overview and purpose

Lateral changes in isostatic gravity across a region result from density changes within rocks of the mid-to-upper crust. Gravity surveys are especially useful in delineating steeply dipping contacts between two rock bodies that have a large contrast in density. Areas of high gravity indicate that high-density rocks (for example many igneous and metamorphic rocks) are closer to the surface. Areas of low gravity indicate less-dense material that results from near-surface low-density sediments, as in sedimentary basins. Gridding gravity measurements creates a map that outlines areas of high gravity and low gravity. Gravity data, paired with other measurable geophysical constraints, allow us to create models of the subsurface that quantitatively predict observed data. When combined with surficial geologic information and density measurements of surficial rocks, gravity can become a powerful modeling tool.

The goals of this gravity survey are to: (1) delineate density contrasts within the subsurface, (2) determine length and geometry of known structures, (3) identify previously unknown structures, and (4) provide geophysical constraints to be used in our forward modeling of the subsurface, which may constrain the geometry of subsurface density contrasts.

Description of method

FIELD METHODS AND SAMPLED LOCATIONS

Data collected with a Lacoste & Romberg G gravimeter (serial # G-908) and Scintrex CG-6 meter (Serial # 19050174), supplement older datasets compiled by Finn and others (1991). We utilized the gravity base stations ‘HEAL’ and ‘ENUM’ to tie our data to the U.S. gravity network. Gravity station spacing at roughly 2 km generates a basic grid over a large area. In areas where known structures exist or initial gravity data collection showed a significant gradient, station spacing is 1 km to provide greater resolution. For modeled cross section lines, station spacing is roughly 250 m along the line, as access warrants. Selecting sites that avoid great topographical relief as much as possible reduces field terrain corrections. Sites with minimal tree cover maximize the effectiveness of the GPS unit (Javad Triumph-2). When tree cover is unavoidable, lengthening the recording time of the GPS unit accordingly provides the best possible vertical accuracy in elevation measurements. Where available, measurements made on exposed bedrock provide ground-truth for map interpretation and modeling. Bedrock density samples and magnetic susceptibility measurements of outcrops constrain geophysical modeling as much as possible at these locations.

DATA REDUCTION AND PROCESSING

A Javad Triumph-2 differential GPS unit provided the horizontal and vertical position of each station. The proprietary Javad Justin software allows for careful data editing and post-processing for differential correction utilizing the National Oceanic and Atmospheric Administration and the National Geodetic Survey’s Continuously Operating Reference Stations (CORS) within 70 km of the study area. After processing, typical positional accuracy is 0.15 m in the vertical and horizontal. Lidar elevation replaces GPS elevation in areas where lidar data is high-resolution and GPS elevation is suspect. We apply the factory instrument (gravimeter) calibration constants to each gravity observation, augmented by correction factors obtained from the Mount Hamilton calibration loop east of San Jose, CA (Barnes and others, 1969), and correcting for Earth tides to produce observed gravity values. The data reference the International Gravity Standardization Net of 1971 (Morelli, 1974) and the reference ellipsoid is the Geodetic Reference System of 1967 (International Union of Geodesy and Geophysics, 1971). The assumed linear drift between base-station ties results in a maximum gravity reading error of 0.05 mGal.

Gravity data reduction formulas for the free-air anomaly are standard (for example, Telford and others, 1990; Swick, 1942) and applying Bouguer, Earth curvature, and terrain corrections out to 166.7 km from each station produces a complete Bouguer anomaly. Terrain corrections are a combination of a field-based component (to a radius of 68 m using the Hayford system; Plouff, 2000) and a computer-generated component (using 30-m USGS DEM digital grids). To assist in the interpretation of mid- to upper-crustal density contrasts, the complete Bouguer anomaly is further reduced to an isostatic anomaly by applying formulas that adjust for long-wavelength variations, such as those caused by the existence of a crustal root and (or) upper-mantle density contrasts. An Airy-Heiskanen model (Heiskanen and Vening-Meinesz, 1958) produces the isostatic correction, assuming a 25-km-thick crust at sea level and a crust-mantle density contrast of 400 kg/m^3. All parts of the data-reduction process assume a standard reduction density of 2,670 kg/m^3. Gravity readings and computed anomalies are in the Data Supplement.

Uncertainties in the gravity data are predominantly due to uncertainty in vertical position and the terrain corrections. Estimating elevation data uncertainties in this study is difficult due to a lack of ground-truthing available. We estimate uncertainties of around 0.15 m on average and a maximum of 1.5 m. This results in an average uncertainty from elevation of 0.03 mGal, up to a maximum of 0.30 mGal. The uncertainty associated with terrain corrections is generally only 5–10 percent of the actual correction. This results in an average terrain-correction uncertainty of 0.08–0.15 mGal but varies according to topography. Average uncertainty

in steep and hilly regions is 0.12–0.23 mGal, whereas average uncertainty in flatter areas is 0.05–0.1 mGal. Based on this, gravity anomalies of 0.5–1 mGal and greater reflect interpretable density variations in the upper crust.

The minimum-curvature algorithms in the GIS software package Geosoft Oasis Montaj transform our point isostatic anomaly data into gridded surfaces. The maximum horizontal gradient (referred to as "max-spots"), calculated using the curvature analysis methodology of Phillips and others (2007), quantitatively locate strong and linear boundaries between rocks in the subsurface that have substantial density differences.

GEOMAGNETICS

Overview and purpose

Magnetic surveys map the changes in the earth's magnetic field due to local magnetic sources at high resolution. This method delineates contacts between geologic units of contrasting magnetic properties, particularly in the mid to upper crust. A large number of magnetic profiles help to precisely determine magnetic contacts and trace them across a map area. Individual profiles, coupled with magnetic susceptibility measurements of surficial rocks, are a powerful geophysical constraint for 2D subsurface modeling.

Aeromagnetics

Aeromagnetic data used in this study were acquired in 1997 (Blakely and others, 1999) via low-flying aircraft with a stinger-mounted magnetometer. North–south flight lines are 0.4 km apart, with east–west tie lines spaced at 8 km. Aeromagnetic measurements were interpolated to a projected, rectilinear grid using a bi-directional gridding algorithm within the GIS software package Geosoft Oasis Montaj. Another filter reduces this anomaly to the magnetic pole, more closely centering anomalies over their sources for map-view interpretation. We apply a filter to the aeromagnetic map to enhance short-wavelength anomalies from shallower sources (termed 'residual'). The residual results from subtracting a version of the original aeromagnetic grid that has been filtered (upward continued 50 m to enhance long-wavelength anomalies) from the original grid. The residual retains short-wavelength anomalies that mainly reflect the effects from sources in the upper couple kilometers of the crust. This method does not produce anomalies reflecting a precise depth of sources, but can separate out anomalies sourced generally deeper or shallower. The same algorithm used to determine the gravity max-spots is applied to either the original, reduced-to-pole, or residual grids to quantitatively locate strong and linear gradients (lineaments) that correspond to sharp and linear subsurface geologic boundaries.

HAND-SAMPLE PROPERTIES

We collected bedrock samples throughout the study area for physical properties laboratory analysis. We weighed samples using an A & D company limited FX-3000i WP analytical balance. Three measurements per sample combine to determine density: a dry weight in air, a submerged (water-saturated) weight, and a water-saturated weight in air. While these measurements produce grain density, saturated bulk density, and dry bulk density, saturated bulk density best reflects subsurface conditions and was therefore referenced for modeling. Magnetic susceptibility measurements taken with a KT10 Kappa Meter accompany rock sample density measurements, and we use the same meter to collect direct readings from outcrops where possible. Weathering tends to replace denser minerals with less dense weathering products and turn magnetite into less magnetic minerals like hematite. Therefore, all of our measured rock densities and susceptibilities from surface outcrops can be considered minimum values; these data are in the Data Supplement.

QUANTITATIVE CROSS-SECTION MODELING

Overview and purpose

Quantitative 2D forward modeling of cross sections constrained by potential-field data provides insight into subsurface unit and fault geometry that goes beyond qualitative interpretations of map-view data. This technique helps provide the best possible interpretation of fault type (for example normal, reverse, or strike-slip), fault dip in the upper crust (for example steep or shallow), and offset across the fault on units with particularly strong physical-property contrasts with surrounding rocks. This method also can identify blind faults that have little surface expression and are difficult to capture via surface geology observations.

Description of method

GM-SYS provides the platform for computing the sum effect of blocks of rock in the subsurface in a 2D cross section on both the gravitational and geomagnetic fields of the Earth. This is a forward-modeling method. This means the operator hypothesizes which rock types are in the subsurface, their location, and their volume, and the GM-SYS program predicts the total fields that result from that particular model. The operator's responsibility is to refine the hypothesis until the predicted potential-fields match the data measured in the field. This ensures that any cross-section interpretation of the subsurface matches two additional data types

(for example gravity and magnetism) besides the geology, and thus reduces the number of potential hypotheses for the subsurface geometry of rocks.

Several lines of data constrain this process in addition to the gravity and aeromagnetic data. Surface geologic observations define rocks that are in the model's near-surface topography, and lab measurements (see above) of density and magnetic properties of hand samples gathered from the surface provide additional rock property constraints. Also essential is the knowledge of the operator and collaborators in the project about the geologic history, expected stratigraphy in the subsurface, and structural geometries that are physically possible based on standard geologic mapping and cross-section construction techniques.

Within these constraints, there is still the strong possibility that multiple hypotheses of subsurface geometry can fit the gravity and magnetic data within the accepted error for those two data types. Therefore, care in the construction of models helps define which parts of the subsurface model are well-constrained with the fewest alternative hypotheses and which parts could have multiple possible geometries. In general, potential-field data provide strong constraint (including their position and dip) on simple, steeply-dipping boundaries that juxtapose rocks with strong differences in physical properties. Potential-field data provide very poor constraint on horizontal boundaries or boundaries between rocks with little contrast in physical properties. Depth of sub-horizontal stratigraphic boundaries within sedimentary rocks is particularly suspect and is never well-constrained without the addition of good quality well or reflection-seismic data. Depth of sub-horizontal boundaries between units of strongly contrasting properties is resolvable but dependent on uncertainties in the physical properties of those units. In those cases, depth of a boundary can trade off with density or magnetism of the rocks.

Our approach first constructs initial simplified models, including uniform packages of sediment, sedimentary rock, metamorphic rock, or volcanic rock to fit the overall long-wavelength features in the gravity and magnetic data. Our model space extends beyond the end of the models shown in this report to avoid edge effects due to truncated subsurface volumes. Adding detail in the stratigraphy and decreasing the size of blocks after the major fit allows modeling of smaller-scale features that fit shorter wavelength anomalies, particularly near the surface. During each iteration, we test possible options for physical properties of rocks and geometries of boundaries permitted by the surface geology observations and measured rock-property constraints. Throughout the process of testing many variables, we conclude that we have a good fit if each model iteration produces a similar solution to fit the data.